Table 2. Observing Bands

Central Wavelength μm	FWHM[a] μm	Band
1.27	0.24	J
1.65	0.32	H
2.23	0.40	K
3.69	0.64	L'
10.6	5.2	N

[a]full width at half maximum of filter

Table 3. 10.6 μm "Standards"

Star B.S. #[a]	[10.6 μm] mag
0337	-2.07
1457	-2.99
1708	-1.95
2491	-1.41
2943	-0.73
2990	-1.24
4069	-1.00
5054	2.24
5340	-3.15
6406	-3.87
7001	0.00
7525	-0.78
8316	-3.84
8775	-2.55

[a]Hoffleit (1964)

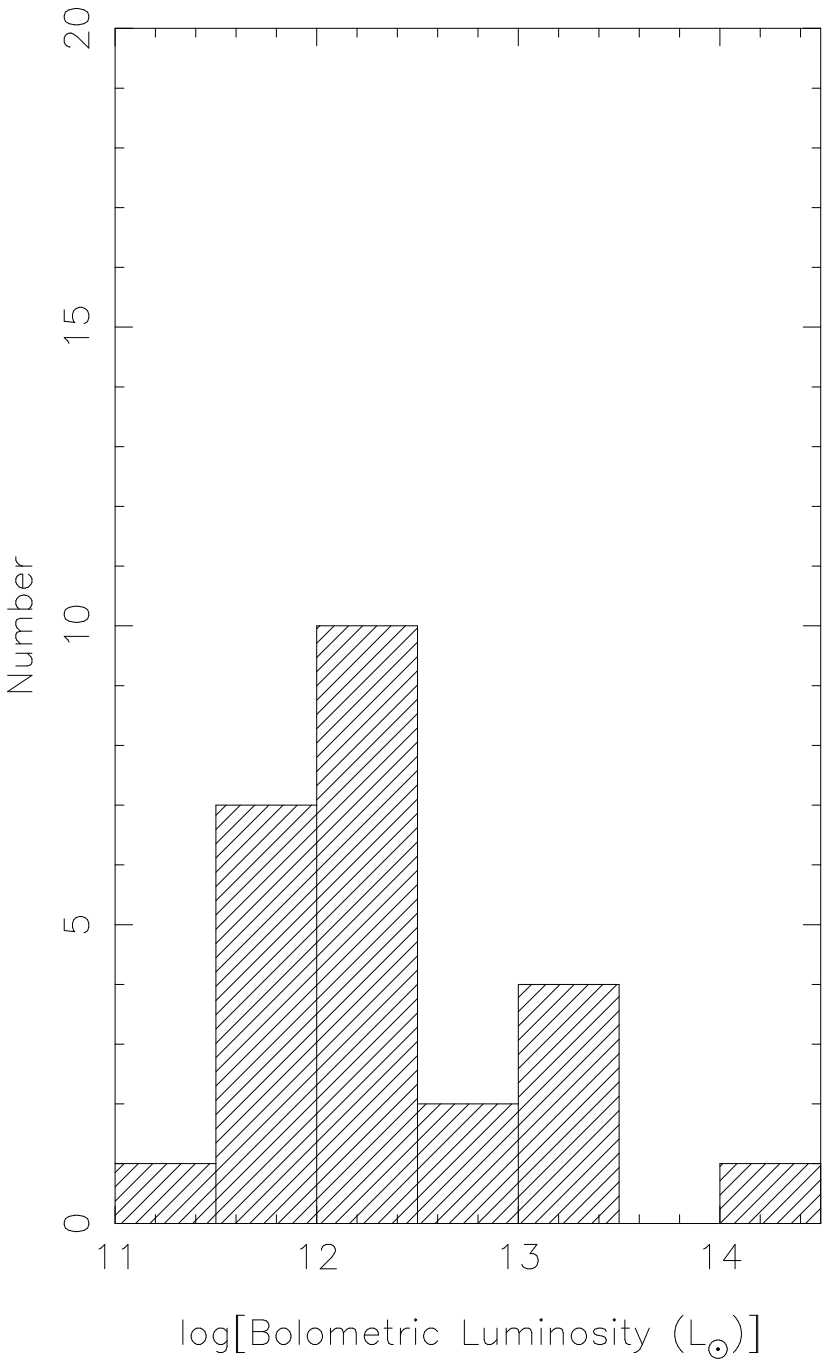
Number
0
5
10
15
20
11
12
13
14
log[Bolometric Luminosity ($L_\odot$)]

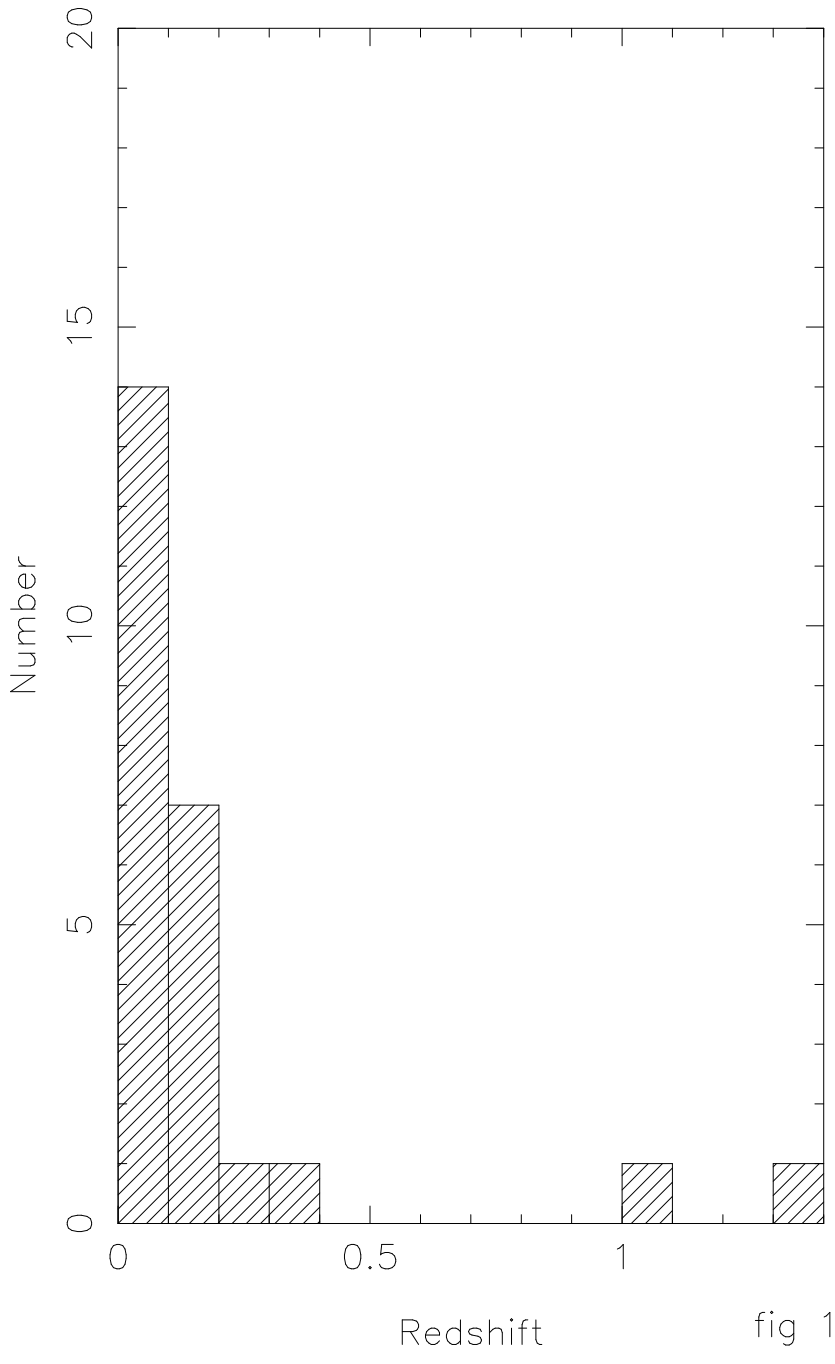
Number
0
5
10
15
20
0
0.5
1
Redshift

fig 1

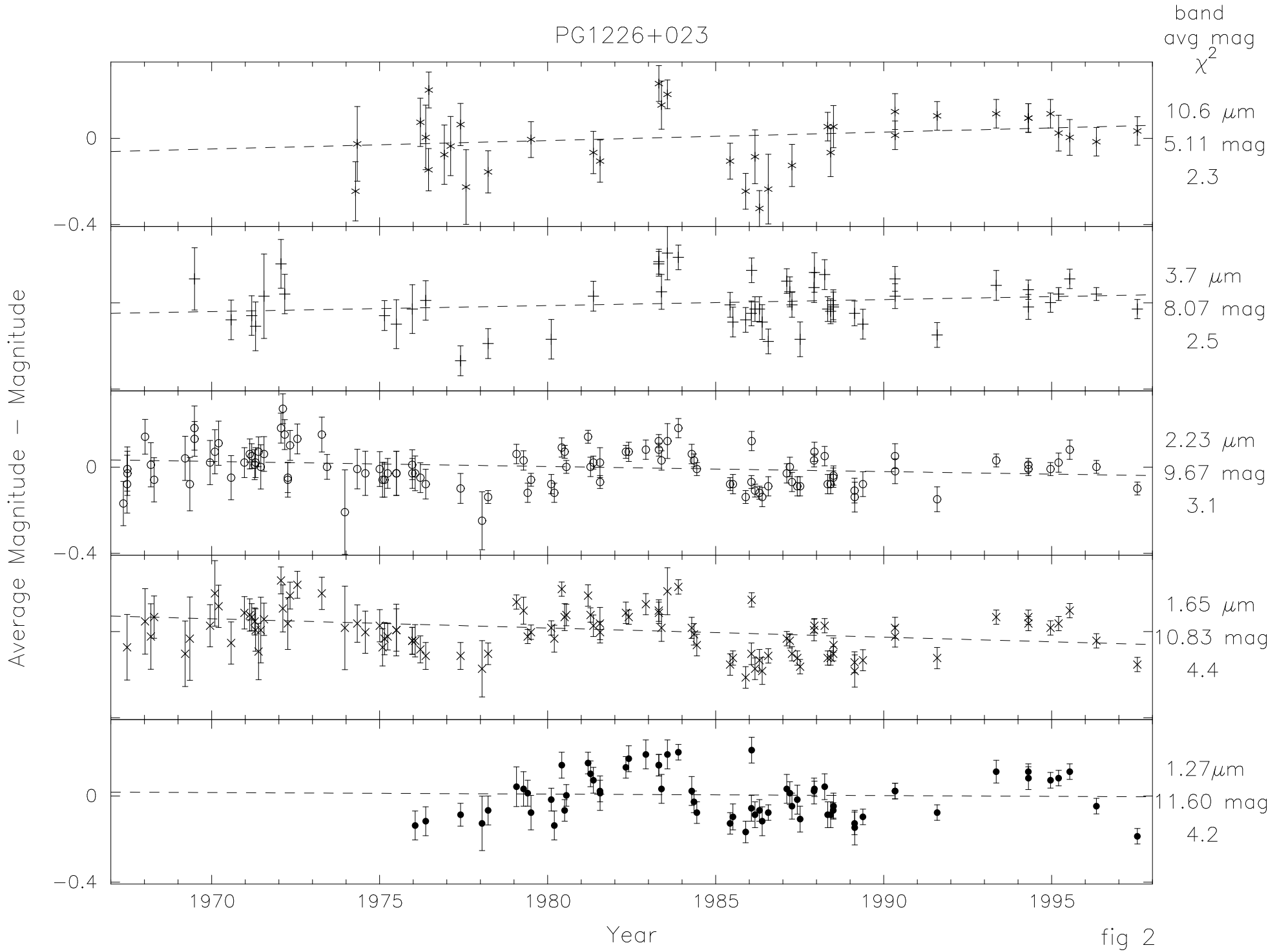
PG1226+023
band
avg mag
χ^2
10.6 μm
5.11 mag
2.3
3.7 μm
8.07 mag
2.5
2.23 μm
9.67 mag
3.1
1.65 μm
10.83 mag
4.4
1.27μm
11.60 mag
4.2
Average Magnitude − Magnitude
0
−0.4
1970
1975
1980
1985
1990
1995
Year

fig 2

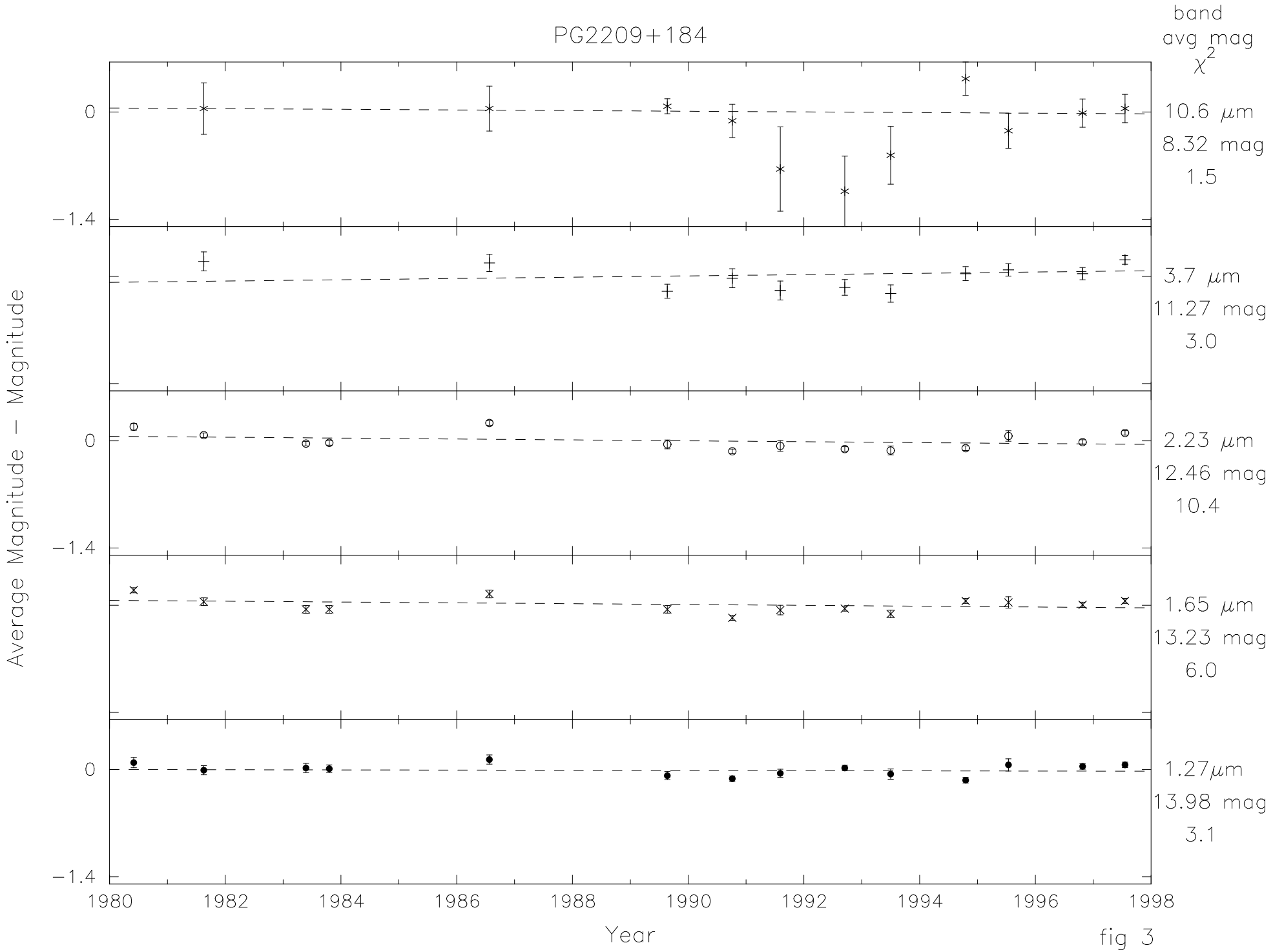
PG2209+184
band
avg mag
χ^2
10.6 μm
8.32 mag
1.5
3.7 μm
11.27 mag
3.0
2.23 μm
12.46 mag
10.4
1.65 μm
13.23 mag
6.0
1.27μm
13.98 mag
3.1
0
−1.4
1980
1982
1984
1986
1988
1990
1992
1994
1996
1998
Year
Average Magnitude − Magnitude

fig 3

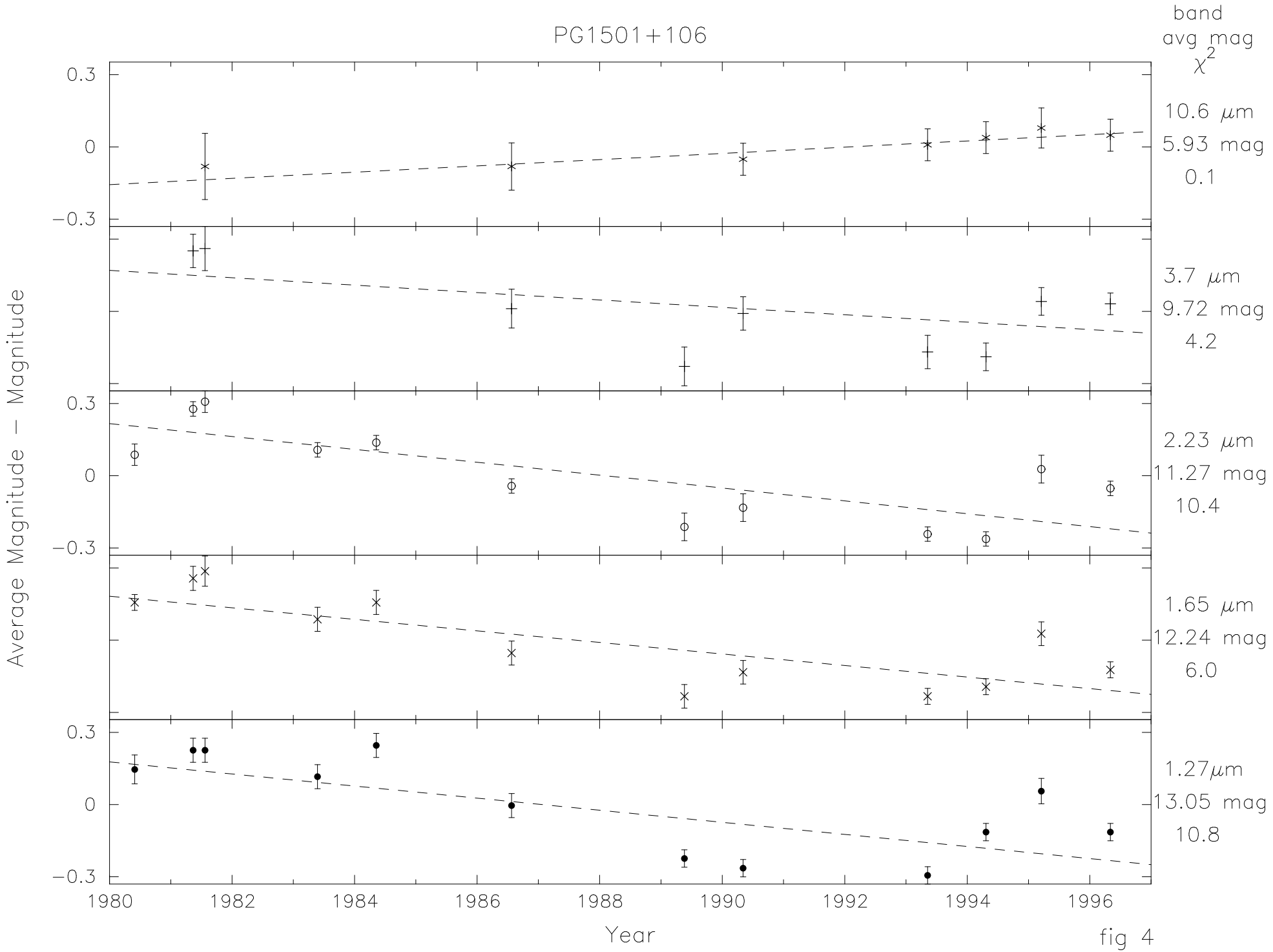
PG1501+106
band
avg mag
χ^2
10.6 μm
5.93 mag
0.1
3.7 μm
9.72 mag
4.2
2.23 μm
11.27 mag
10.4
1.65 μm
12.24 mag
6.0
1.27μm
13.05 mag
10.8
Average Magnitude − Magnitude
0.3
0
−0.3
1980
1982
1984
1986
1988
1990
1992
1994
1996
Year

fig 4

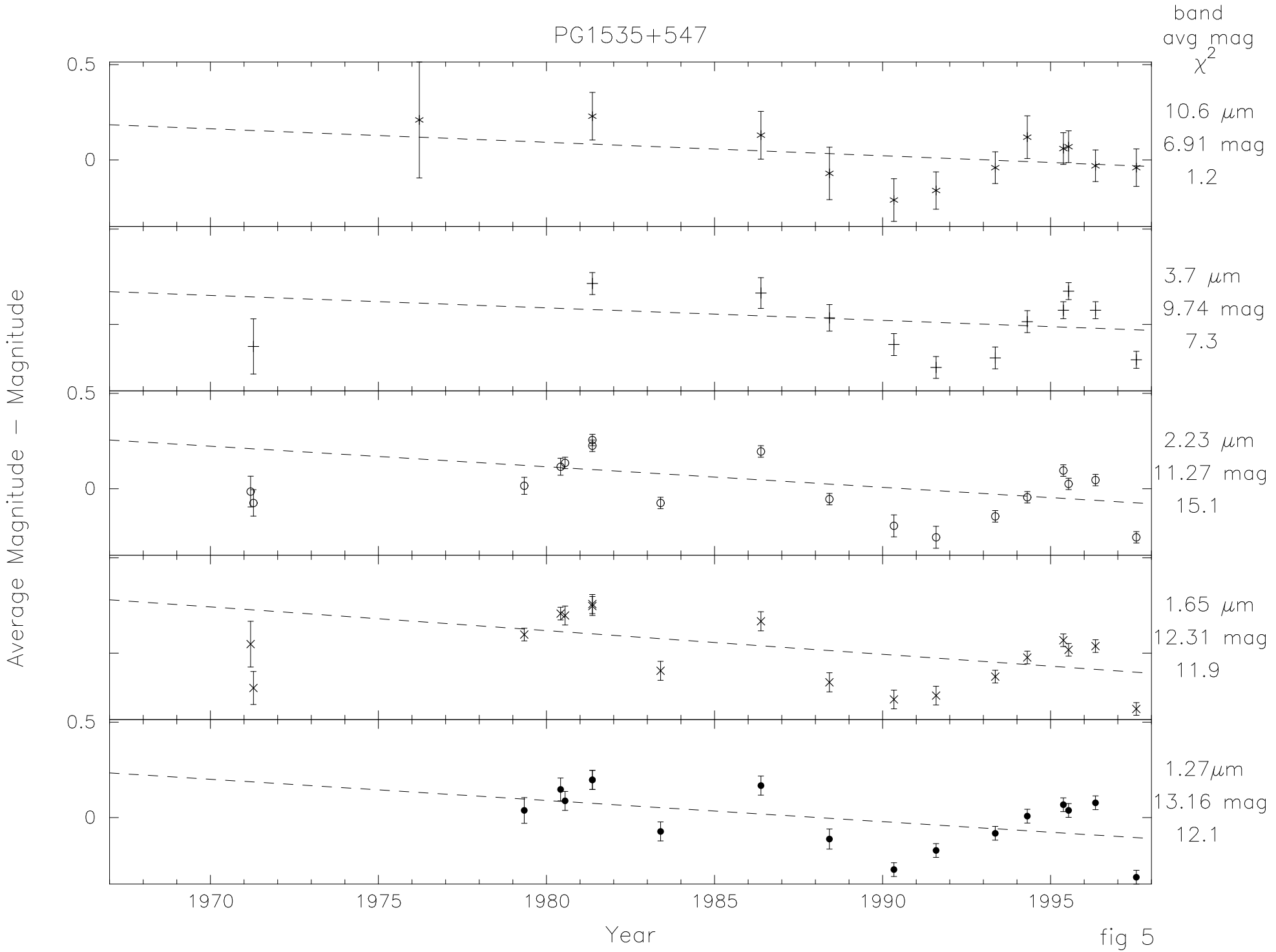
PG1535+547
band
avg mag
χ^2
10.6 μm
6.91 mag
1.2
3.7 μm
9.74 mag
7.3
2.23 μm
11.27 mag
15.1
1.65 μm
12.31 mag
11.9
1.27μm
13.16 mag
12.1
0.5
0
Average Magnitude − Magnitude
1970
1975
1980
1985
1990
1995
Year

fig 5

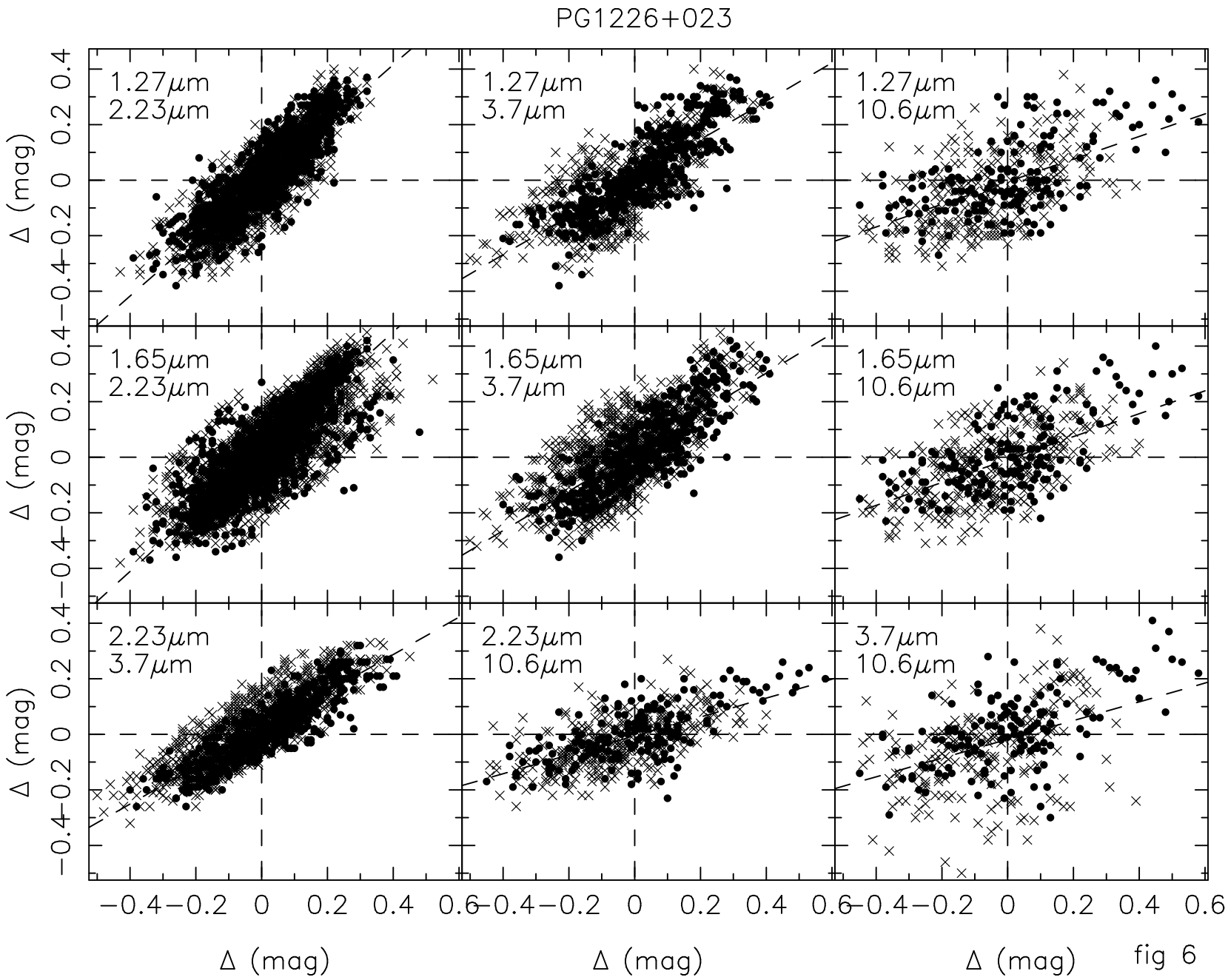
PG1226+023
1.27μm
2.23μm
1.27μm
3.7μm
1.27μm
10.6μm
1.65μm
2.23μm
1.65μm
3.7μm
1.65μm
10.6μm
2.23μm
3.7μm
2.23μm
10.6μm
3.7μm
10.6μm
Δ (mag)
−0.4 −0.2 0 0.2 0.4 0.6

fig 6

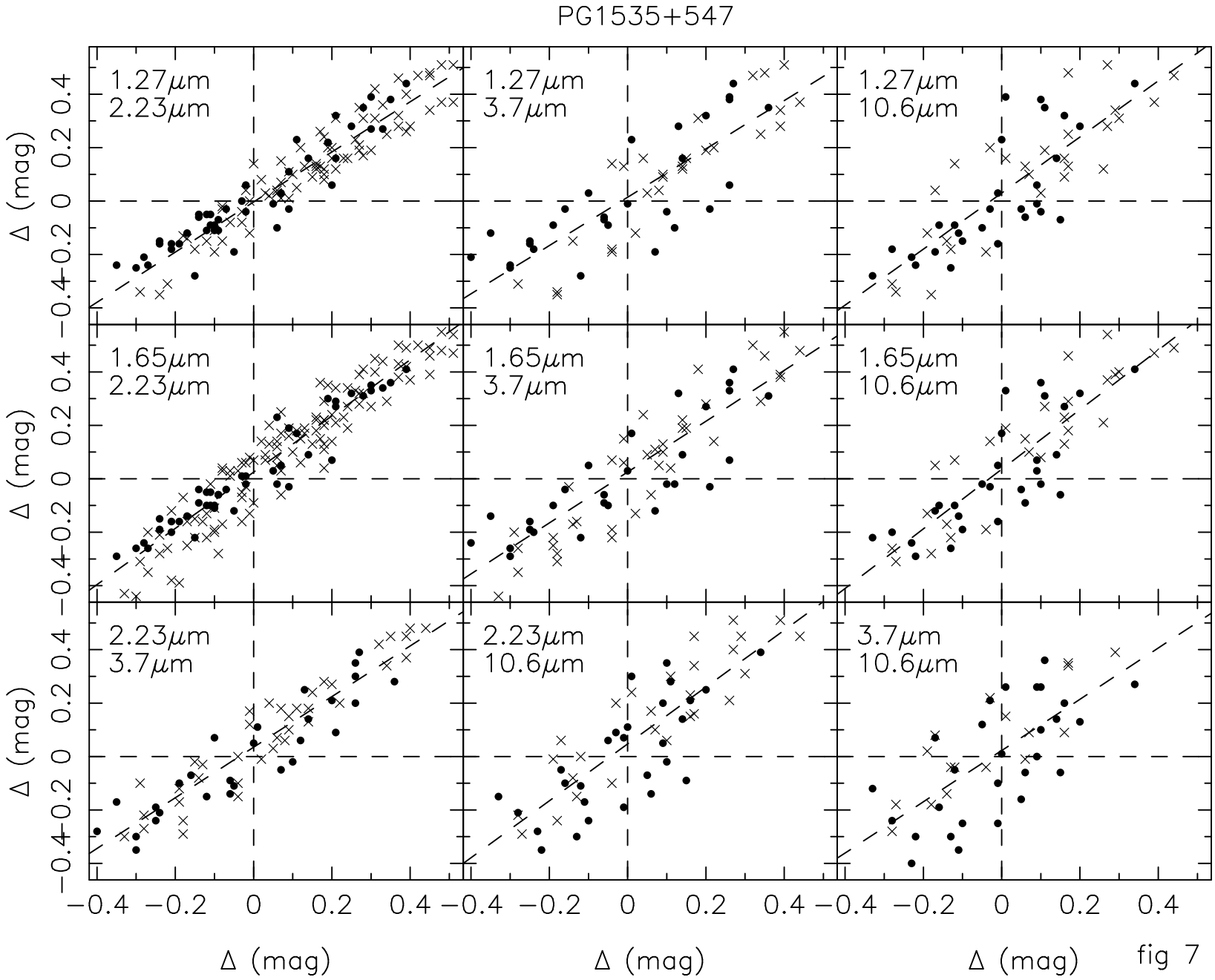
PG1535+547
1.27μm
2.23μm
1.27μm
3.7μm
1.27μm
10.6μm
1.65μm
2.23μm
1.65μm
3.7μm
1.65μm
10.6μm
2.23μm
3.7μm
2.23μm
10.6μm
3.7μm
10.6μm
Δ (mag)
−0.4 −0.2 0 0.2 0.4

fig 7

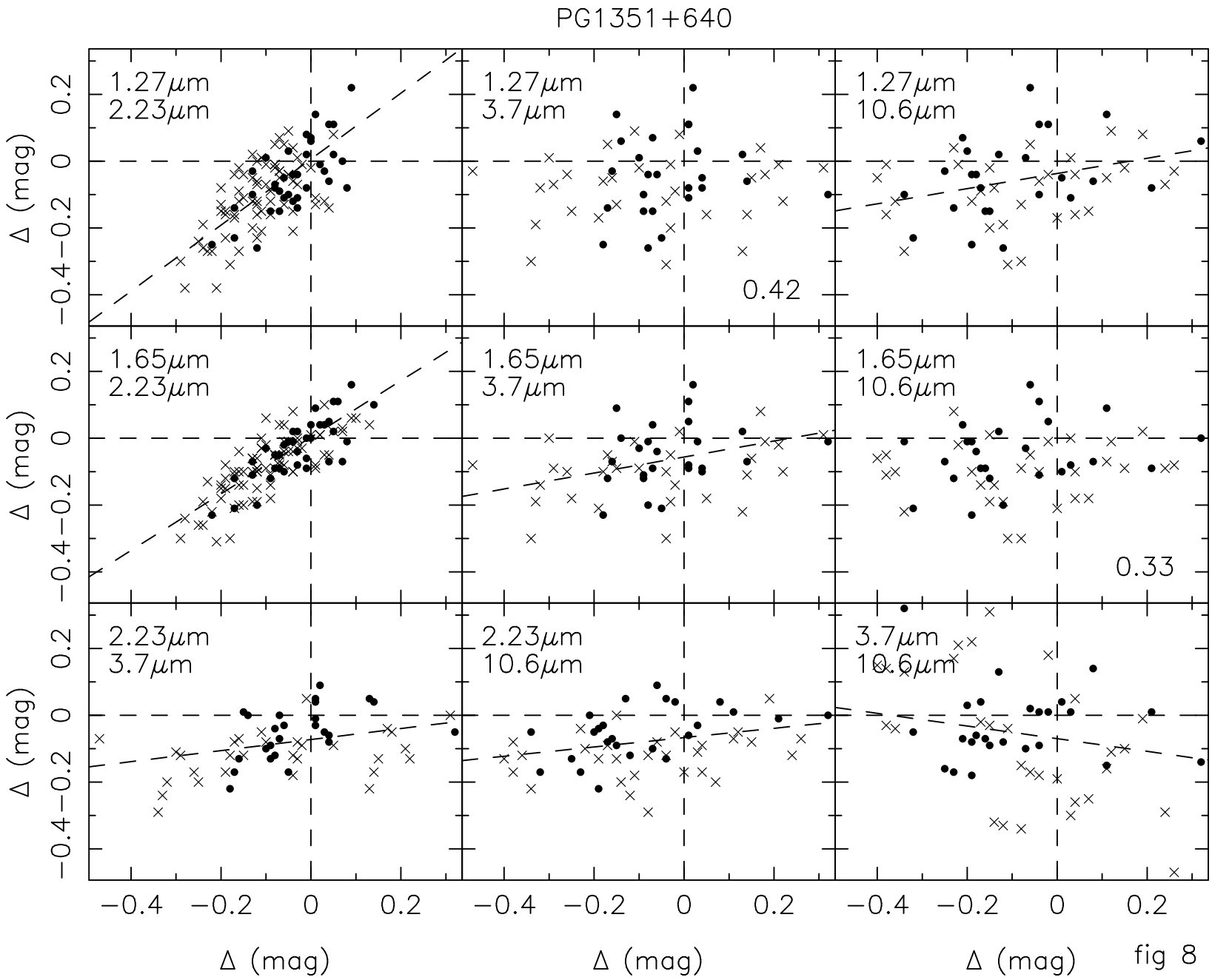
PG1351+640
1.27μm
2.23μm
1.27μm
3.7μm
0.42
1.27μm
10.6μm
1.65μm
2.23μm
1.65μm
3.7μm
1.65μm
10.6μm
0.33
2.23μm
3.7μm
2.23μm
10.6μm
3.7μm
10.6μm
Δ (mag)
−0.4
−0.2
0
0.2

fig 8

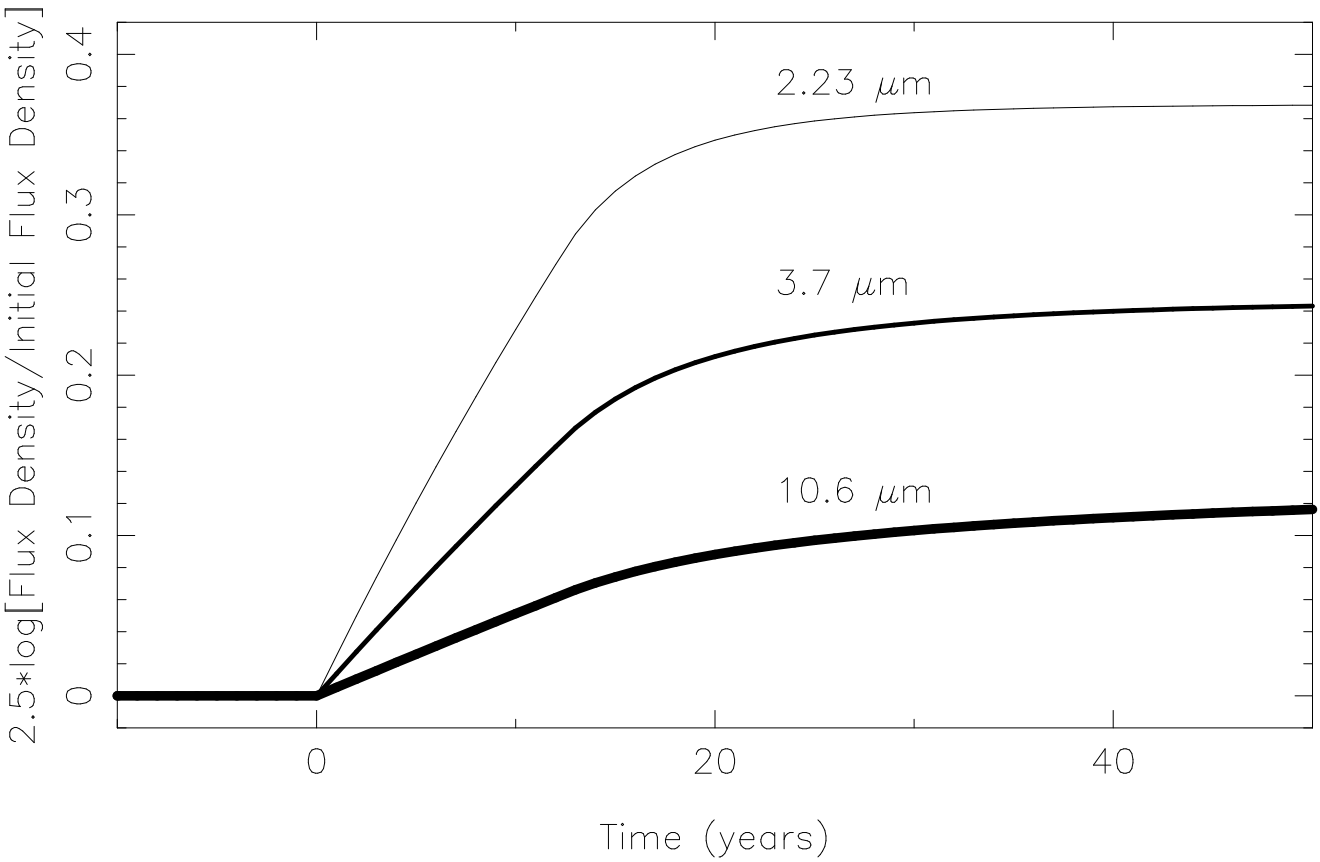
2.5*log[Flux Density/Initial Flux Density]
0
0.1
0.2
0.3
0.4
2.23 μm
3.7 μm
10.6 μm
0
20
40
Time (years)

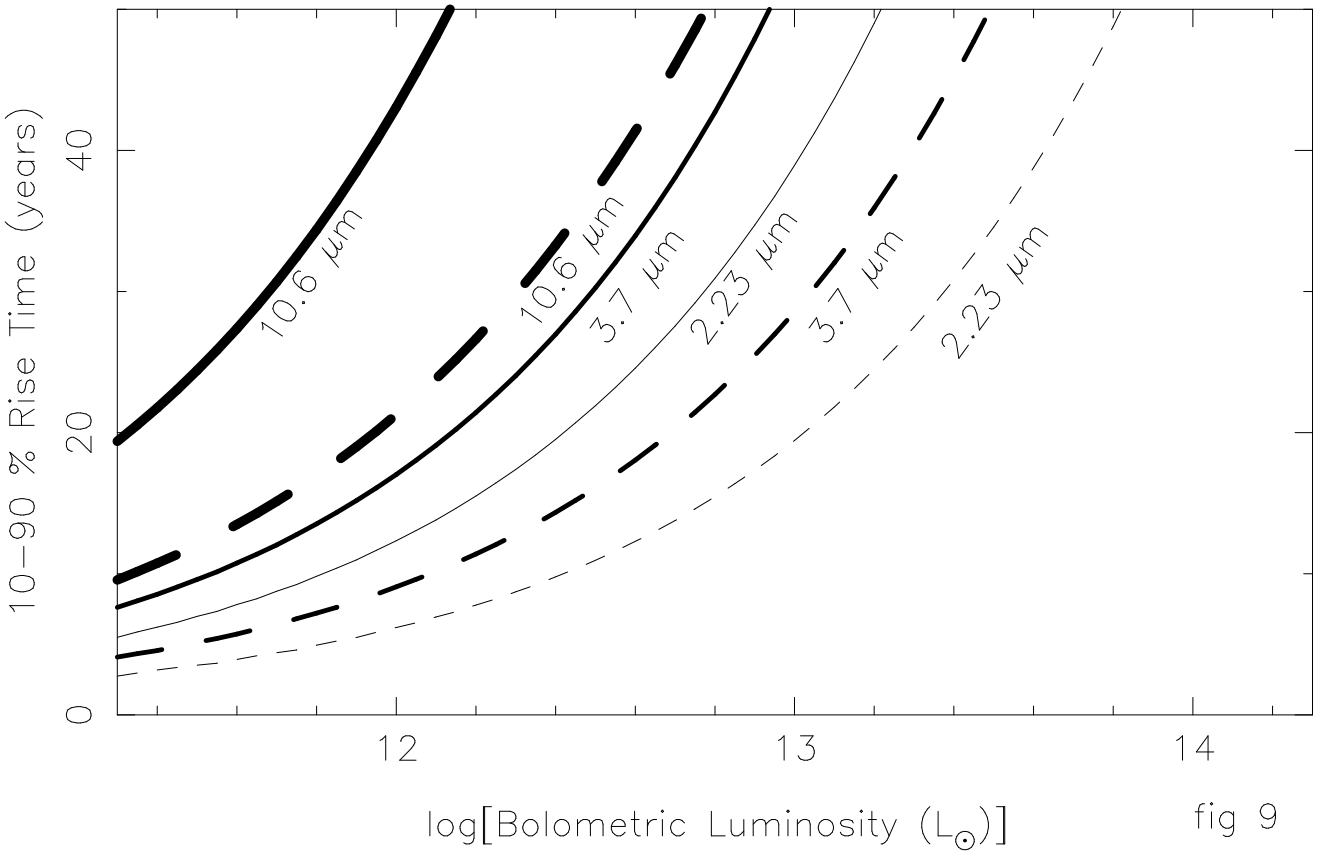
10−90 % Rise Time (years)
0
20
40
10.6 μm
10.6 μm
3.7 μm
2.23 μm
3.7 μm
2.23 μm
12
13
14
log[Bolometric Luminosity (L⊙)]

fig 9

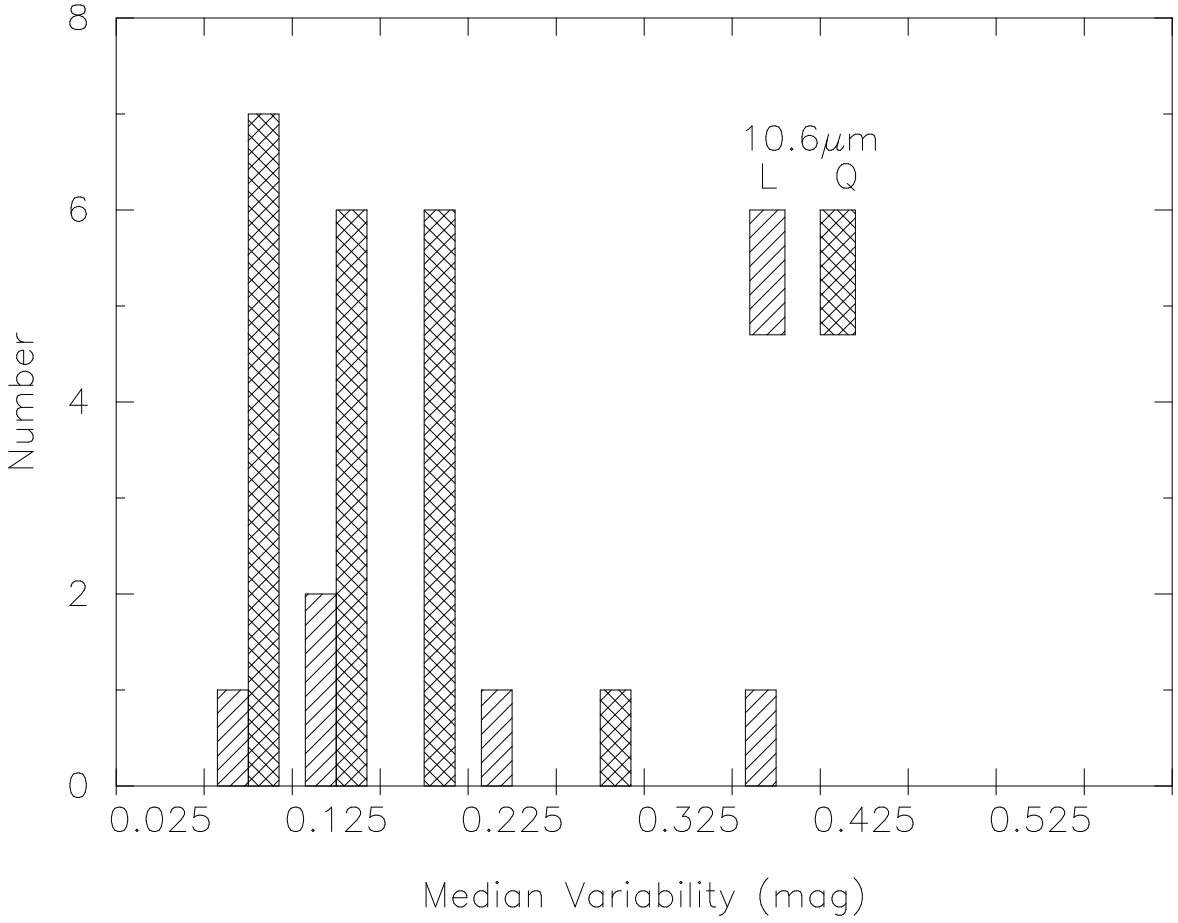
10.6μm
L Q
Number
Median Variability (mag)
0
2
4
6
8
0.025
0.125
0.225
0.325
0.425
0.525

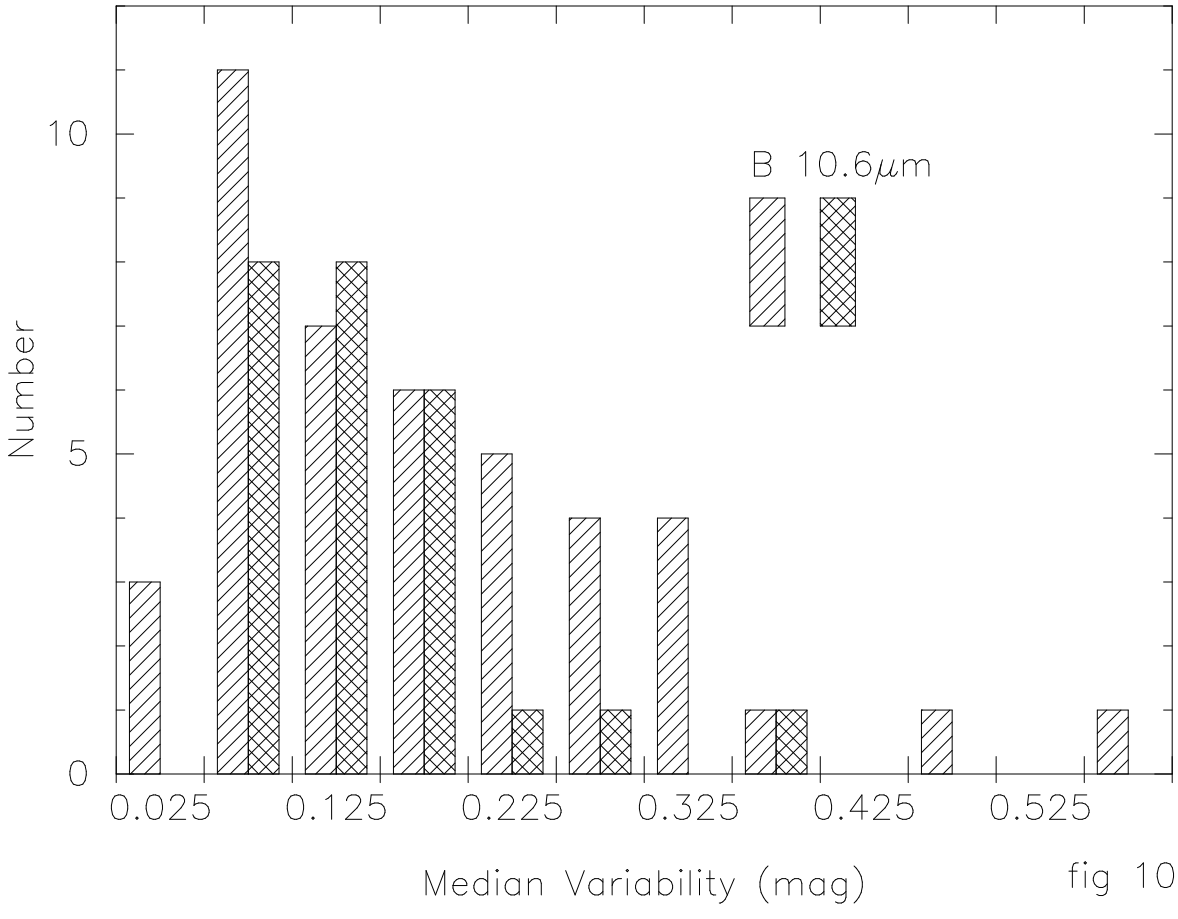
B 10.6μm
Number
Median Variability (mag)
0
5
10
0.025
0.125
0.225
0.325
0.425
0.525

fig 10

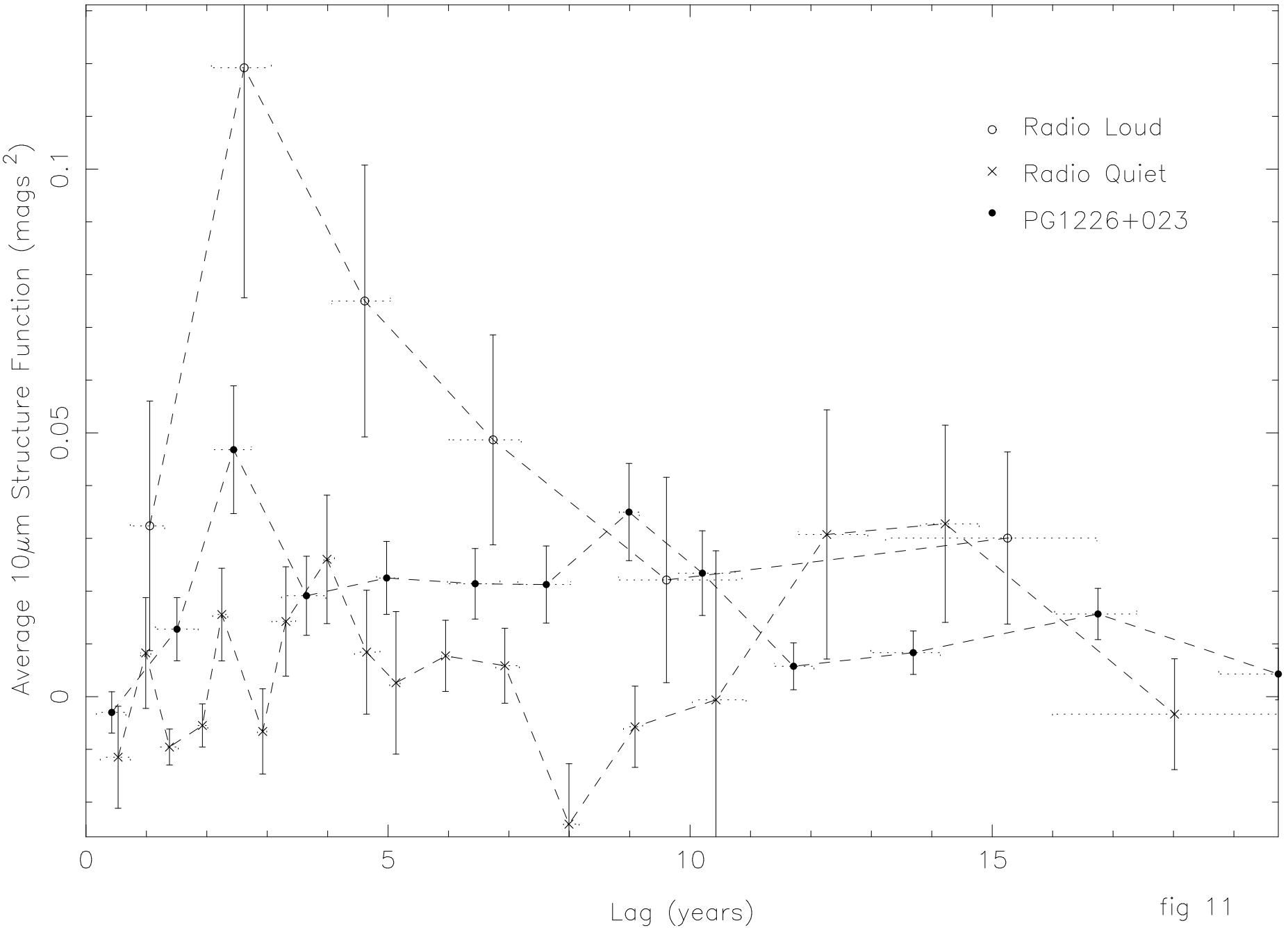
Radio Loud
Radio Quiet
PG1226+023
Average 10μm Structure Function (mags^2)
0
0.05
0.1
0
5
10
15
Lag (years)

fig 11

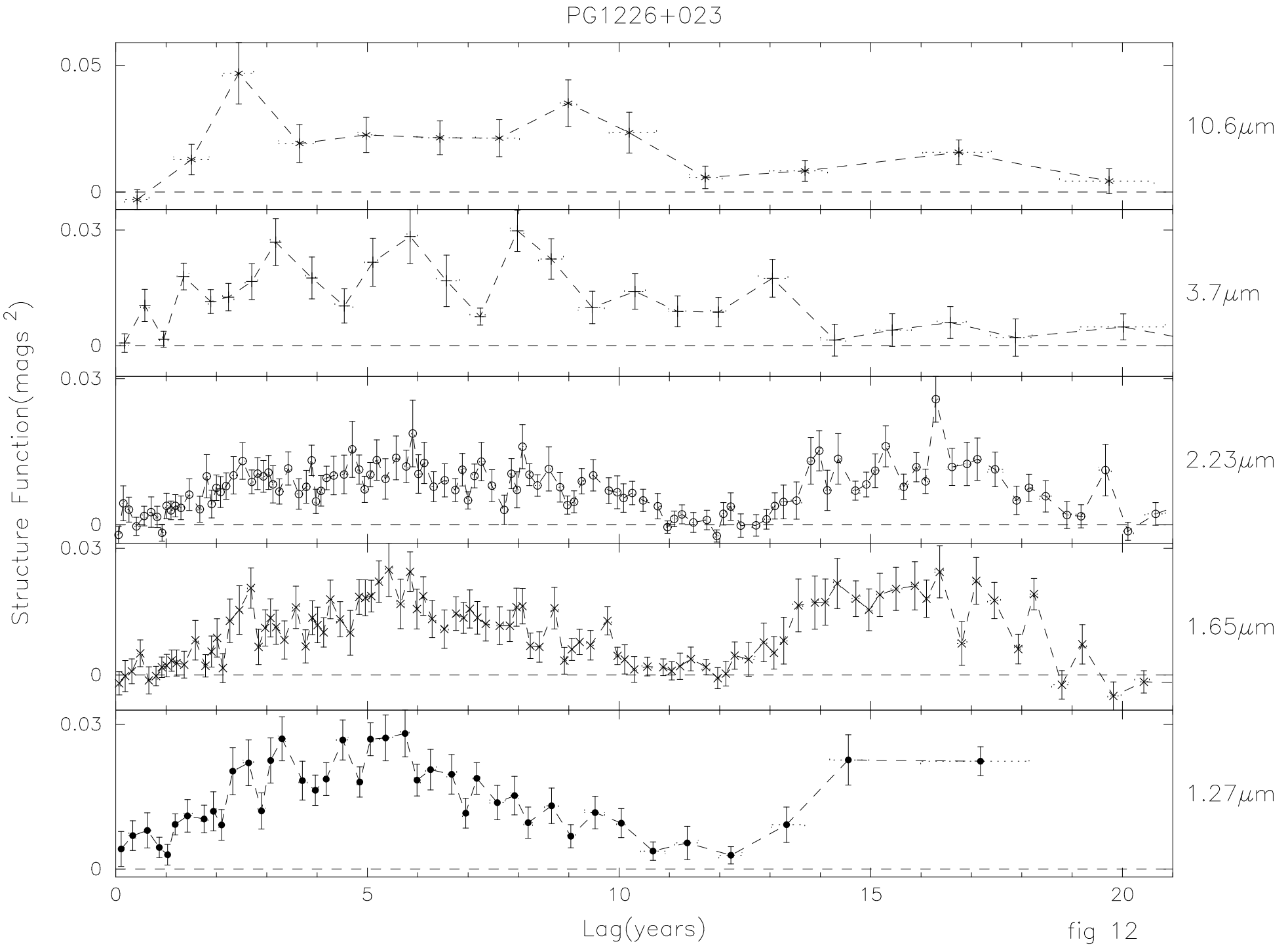
PG1226+023
0.05
0
10.6μm
0.03
0
3.7μm
0.03
0
2.23μm
0.03
0
1.65μm
0.03
0
1.27μm
Structure Function(mags 2)
0
5
10
15
20
Lag(years)

fig 12

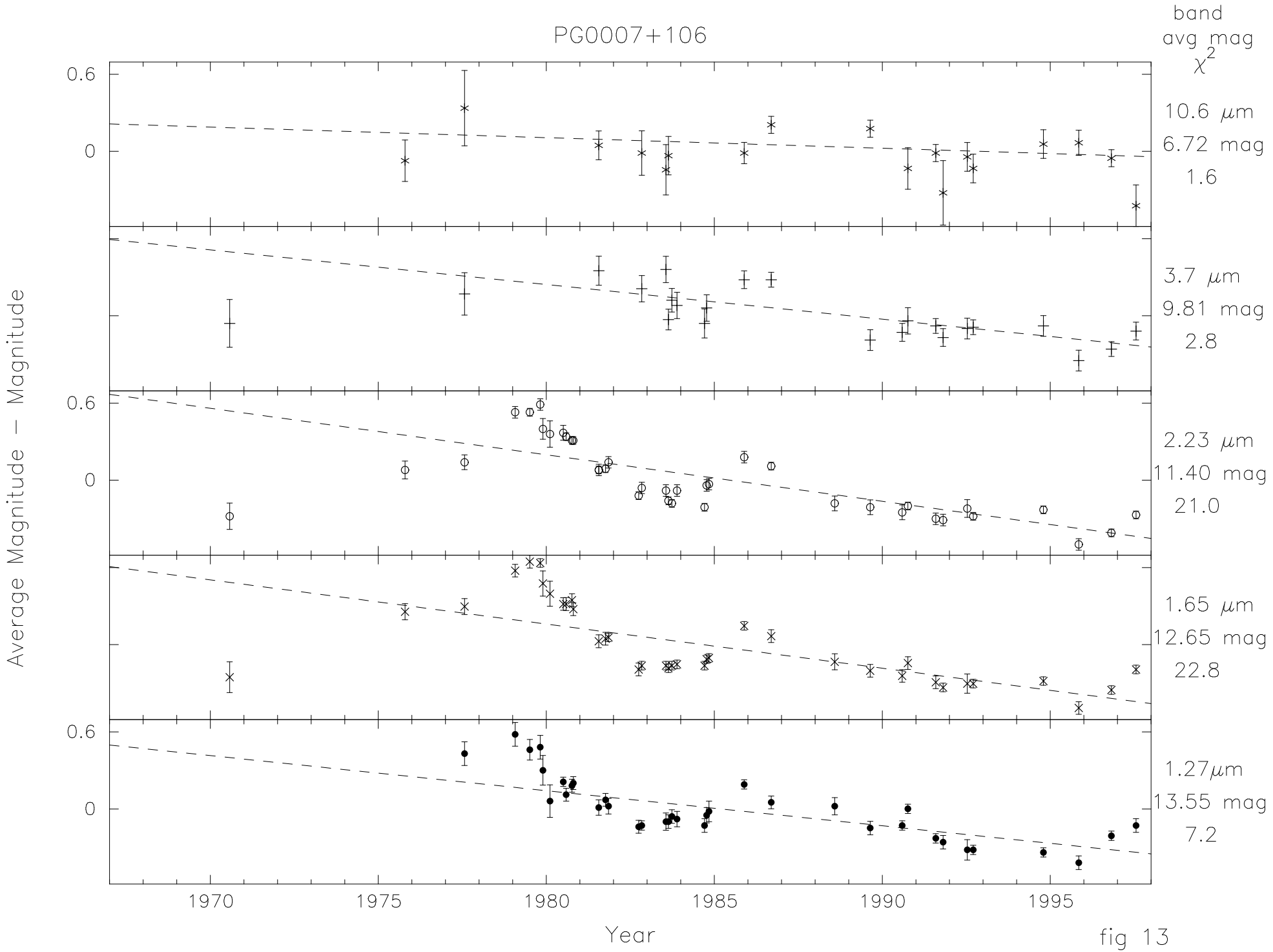
PG0007+106
band
avg mag
χ^2
10.6 μm
6.72 mag
1.6
3.7 μm
9.81 mag
2.8
2.23 μm
11.40 mag
21.0
1.65 μm
12.65 mag
22.8
1.27μm
13.55 mag
7.2
0.6
0
Average Magnitude − Magnitude
1970
1975
1980
1985
1990
1995
Year

fig 13

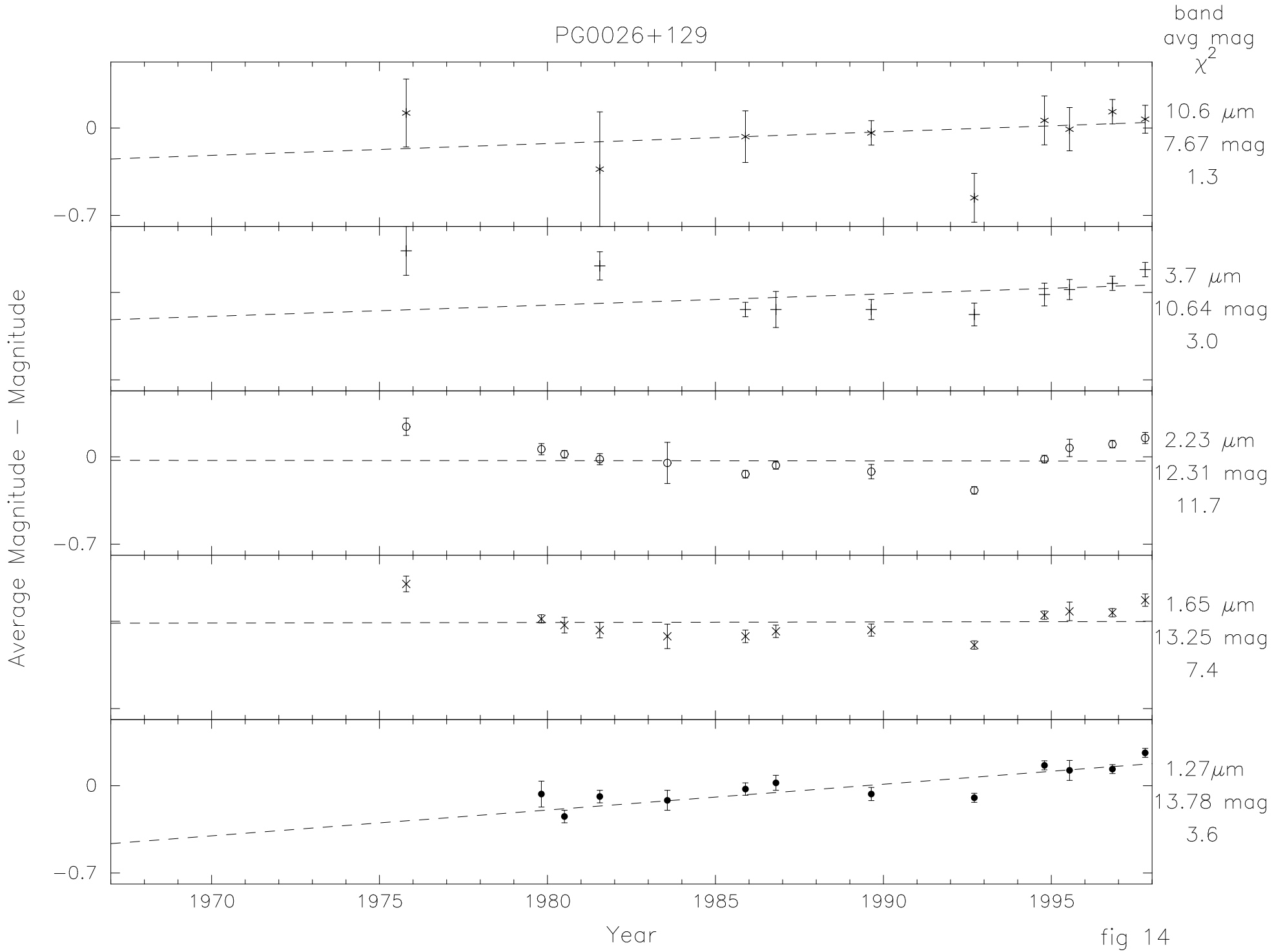
PG0026+129
band
avg mag
χ^2
10.6 μm
7.67 mag
1.3
3.7 μm
10.64 mag
3.0
2.23 μm
12.31 mag
11.7
1.65 μm
13.25 mag
7.4
1.27μm
13.78 mag
3.6
0
−0.7
Average Magnitude − Magnitude
1970
1975
1980
1985
1990
1995
Year

fig 14

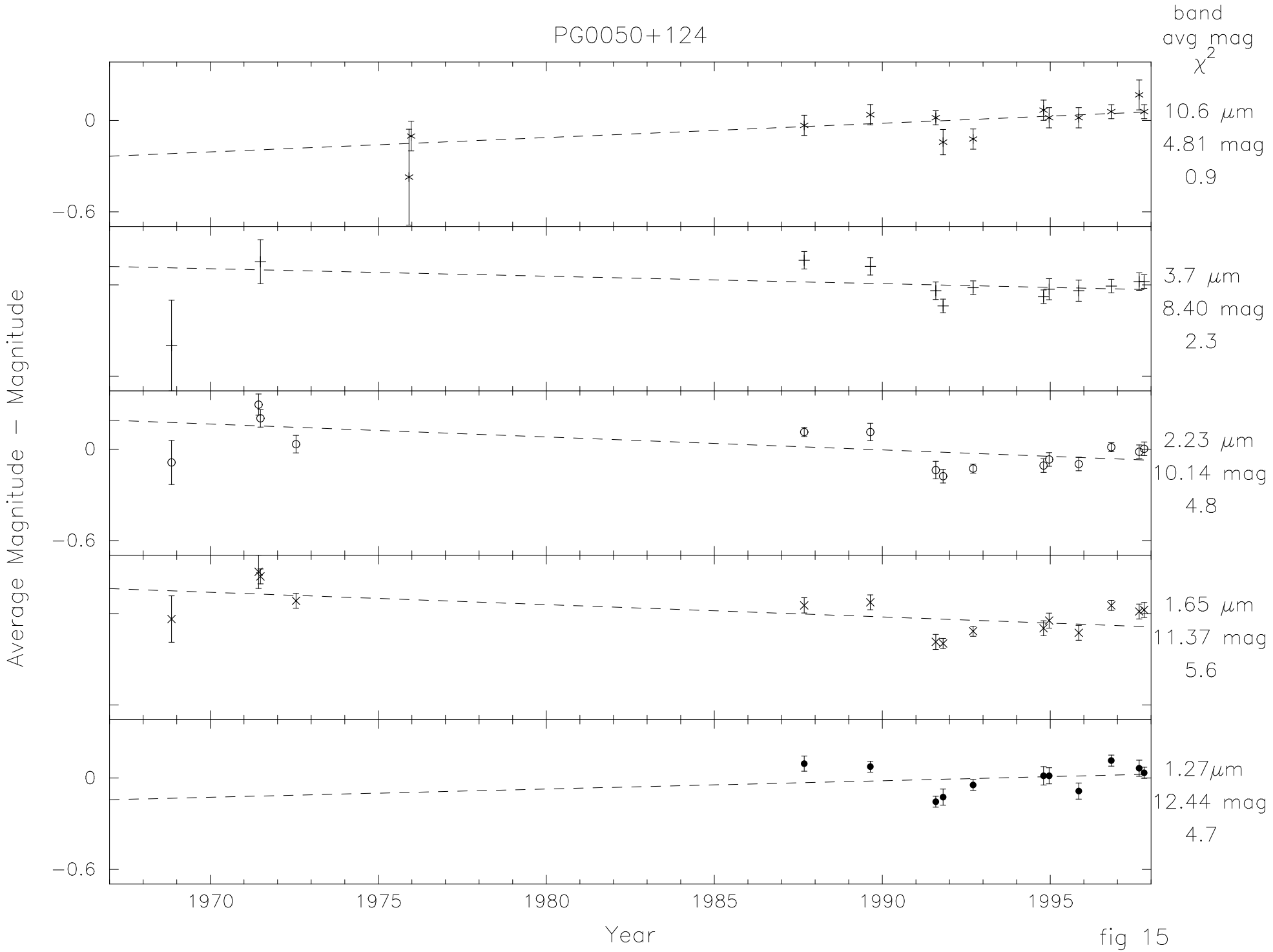
PG0050+124
band
avg mag
χ^2
10.6 μm
4.81 mag
0.9
3.7 μm
8.40 mag
2.3
2.23 μm
10.14 mag
4.8
1.65 μm
11.37 mag
5.6
1.27μm
12.44 mag
4.7
0
−0.6
Average Magnitude − Magnitude
1970
1975
1980
1985
1990
1995
Year

fig 15

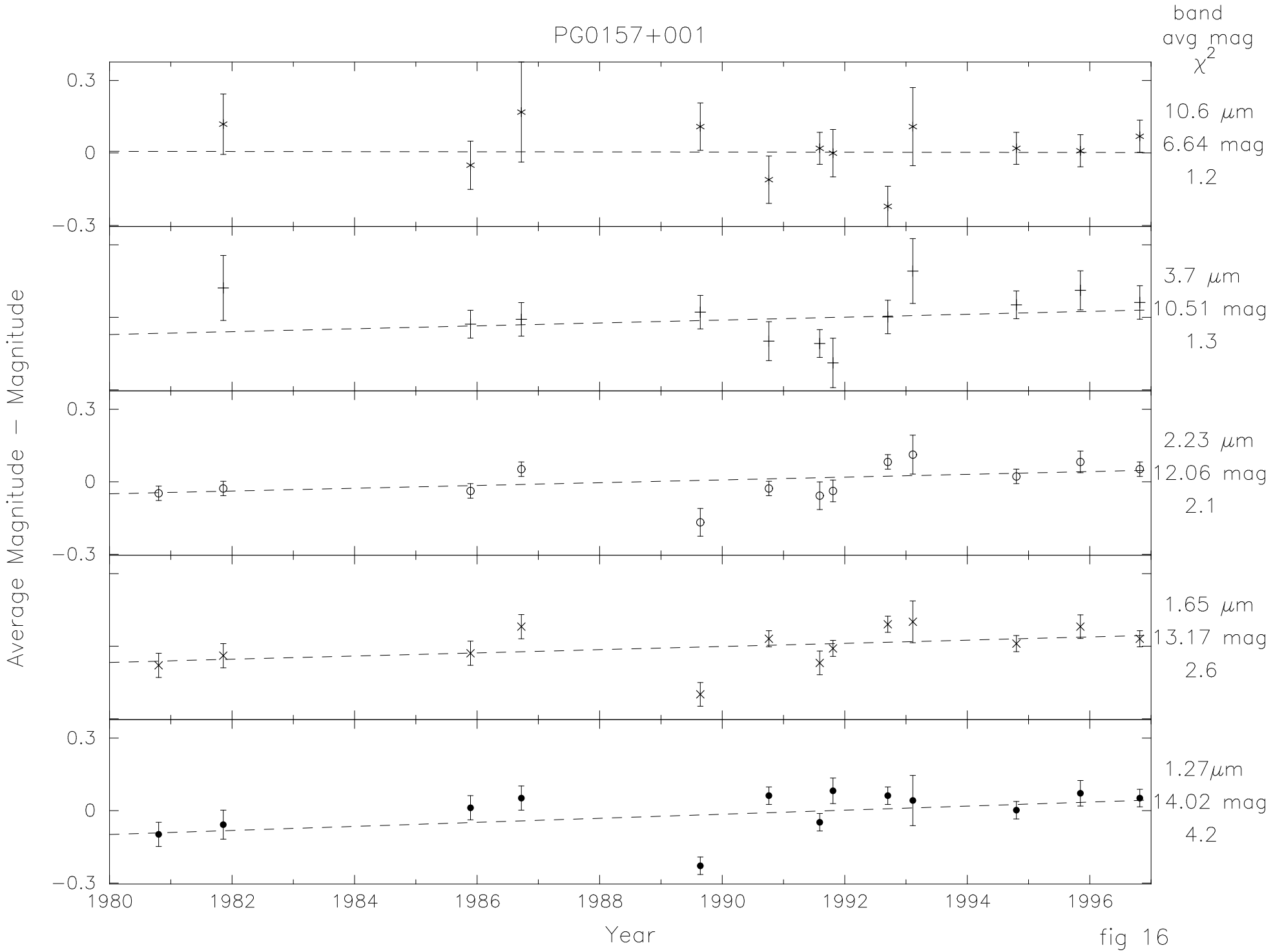
PG0157+001
band
avg mag
χ^2
10.6 μm
6.64 mag
1.2
3.7 μm
10.51 mag
1.3
2.23 μm
12.06 mag
2.1
1.65 μm
13.17 mag
2.6
1.27μm
14.02 mag
4.2
0.3
0
−0.3
1980
1982
1984
1986
1988
1990
1992
1994
1996
Year
Average Magnitude − Magnitude

fig 16

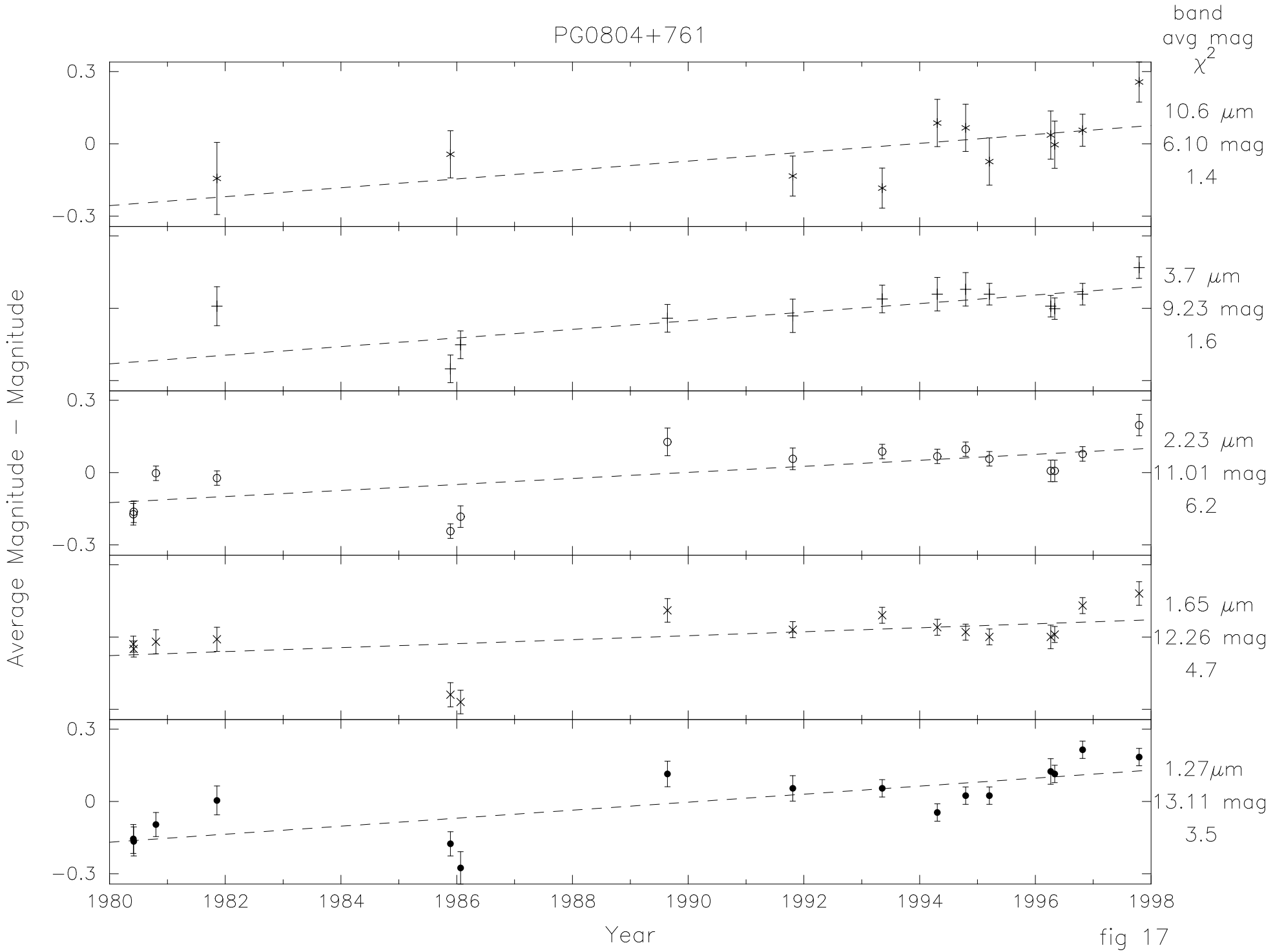
PG0804+761
band
avg mag
χ^2
10.6 μm
6.10 mag
1.4
3.7 μm
9.23 mag
1.6
2.23 μm
11.01 mag
6.2
1.65 μm
12.26 mag
4.7
1.27μm
13.11 mag
3.5
0.3
0
−0.3
1980
1982
1984
1986
1988
1990
1992
1994
1996
1998
Year
Average Magnitude − Magnitude

fig 17

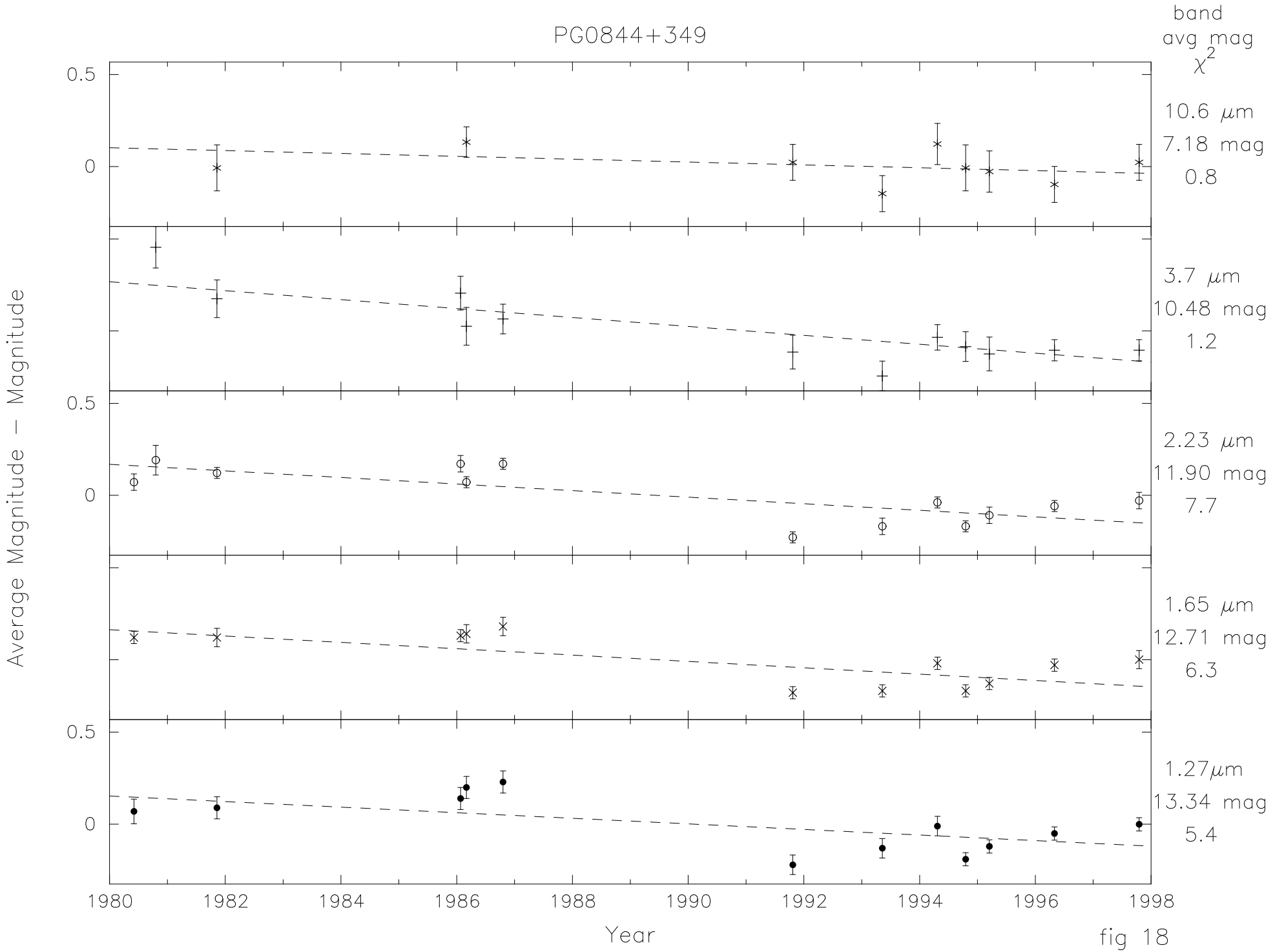
PG0844+349
band
avg mag
χ^2
10.6 μm
7.18 mag
0.8
3.7 μm
10.48 mag
1.2
2.23 μm
11.90 mag
7.7
1.65 μm
12.71 mag
6.3
1.27μm
13.34 mag
5.4
0.5
0
1980
1982
1984
1986
1988
1990
1992
1994
1996
1998
Year
Average Magnitude − Magnitude

fig 18

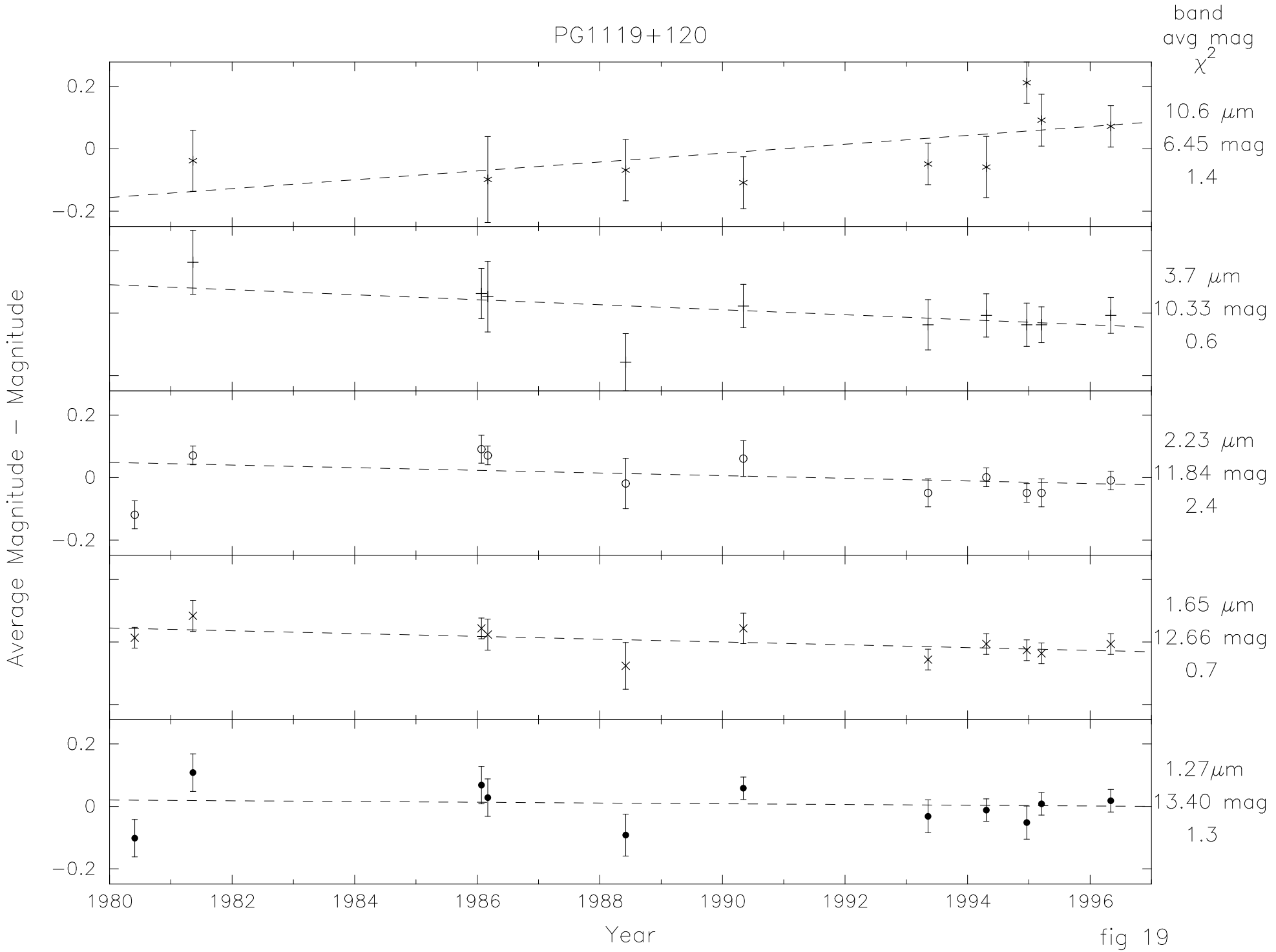
PG1119+120
band
avg mag
χ^2
10.6 μm
6.45 mag
1.4
3.7 μm
10.33 mag
0.6
2.23 μm
11.84 mag
2.4
1.65 μm
12.66 mag
0.7
1.27μm
13.40 mag
1.3
0.2
0
−0.2
1980
1982
1984
1986
1988
1990
1992
1994
1996
Year
Average Magnitude − Magnitude

fig 19

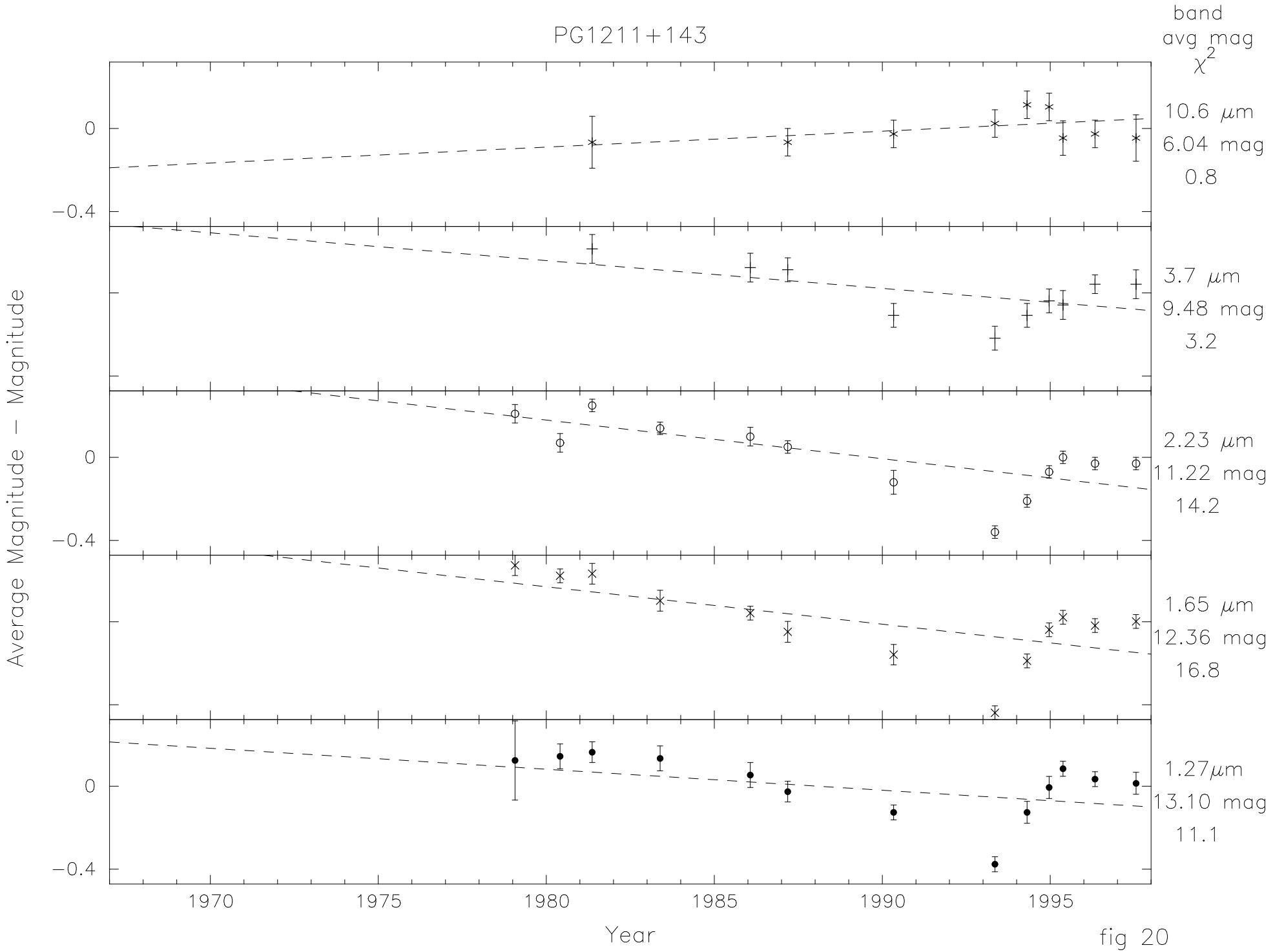
PG1211+143
band
avg mag
χ^2
10.6 μm
6.04 mag
0.8
3.7 μm
9.48 mag
3.2
2.23 μm
11.22 mag
14.2
1.65 μm
12.36 mag
16.8
1.27μm
13.10 mag
11.1
0
−0.4
Average Magnitude − Magnitude
1970
1975
1980
1985
1990
1995
Year

fig 20

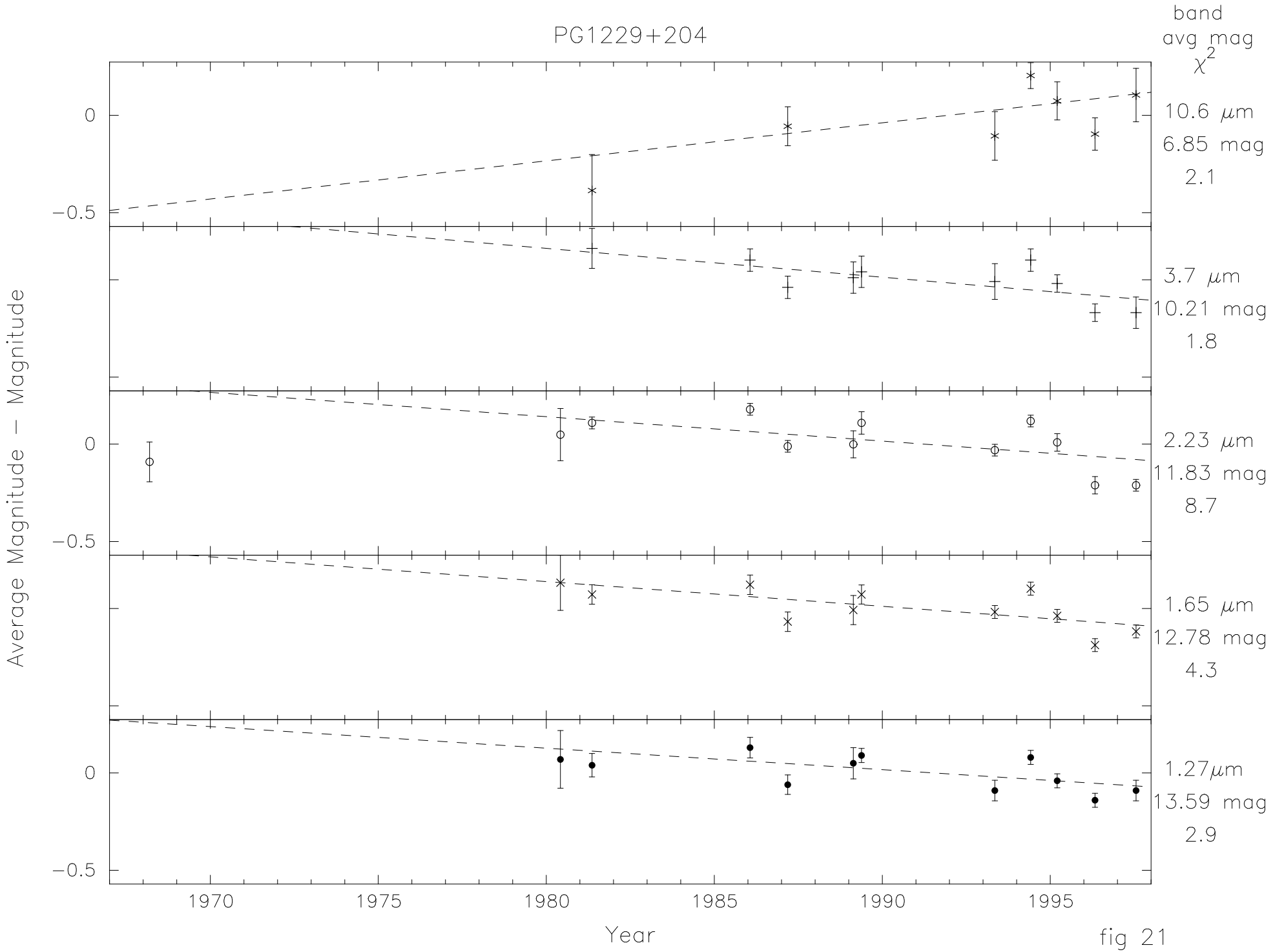
PG1229+204
band
avg mag
χ^2
10.6 μm
6.85 mag
2.1
3.7 μm
10.21 mag
1.8
2.23 μm
11.83 mag
8.7
1.65 μm
12.78 mag
4.3
1.27μm
13.59 mag
2.9
0
−0.5
Average Magnitude − Magnitude
1970
1975
1980
1985
1990
1995
Year

fig 21

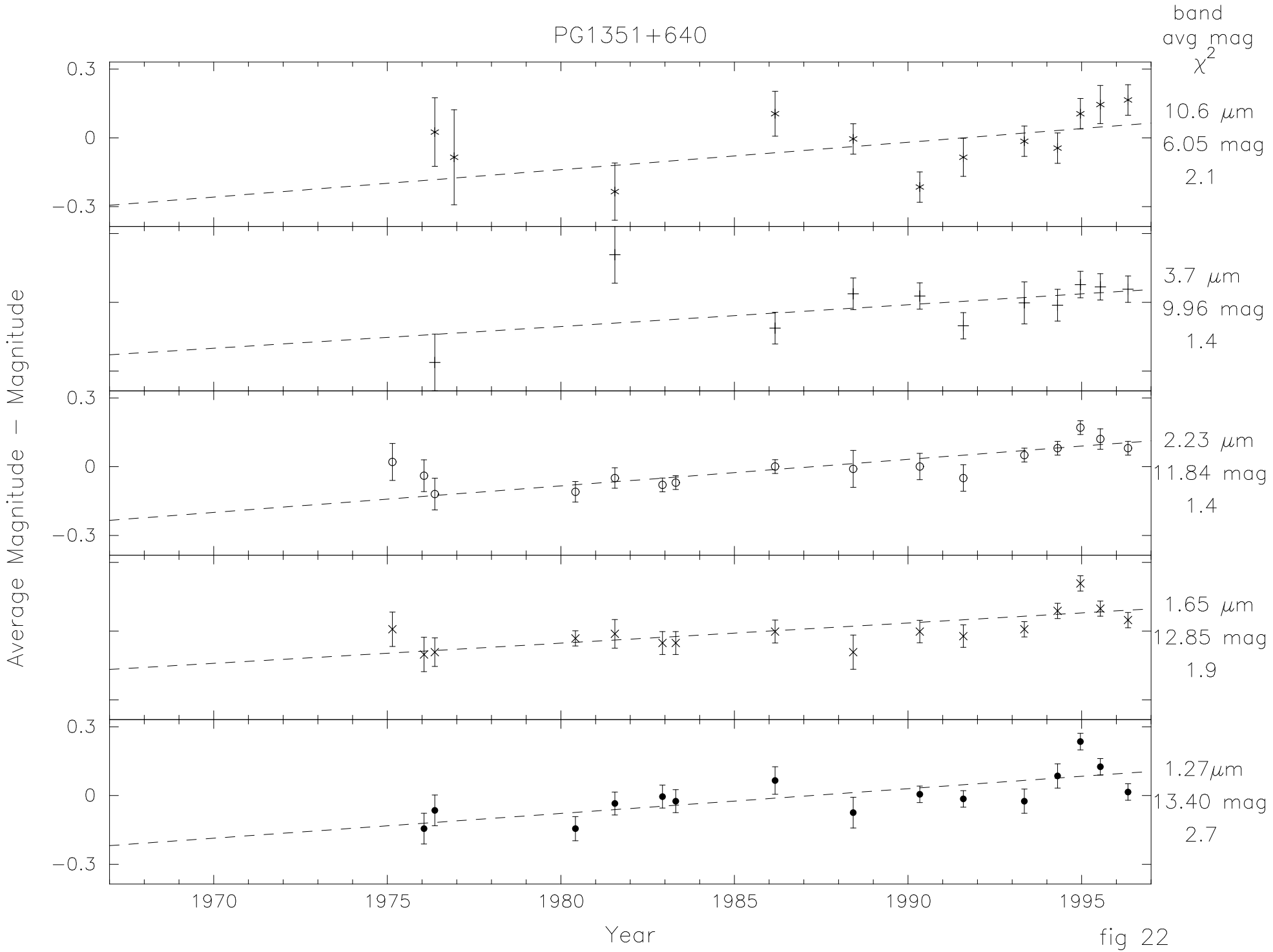
PG1351+640
band
avg mag
χ^2
10.6 μm
6.05 mag
2.1
3.7 μm
9.96 mag
1.4
2.23 μm
11.84 mag
1.4
1.65 μm
12.85 mag
1.9
1.27μm
13.40 mag
2.7
0.3
0
−0.3
1970
1975
1980
1985
1990
1995
Year
Average Magnitude − Magnitude

fig 22

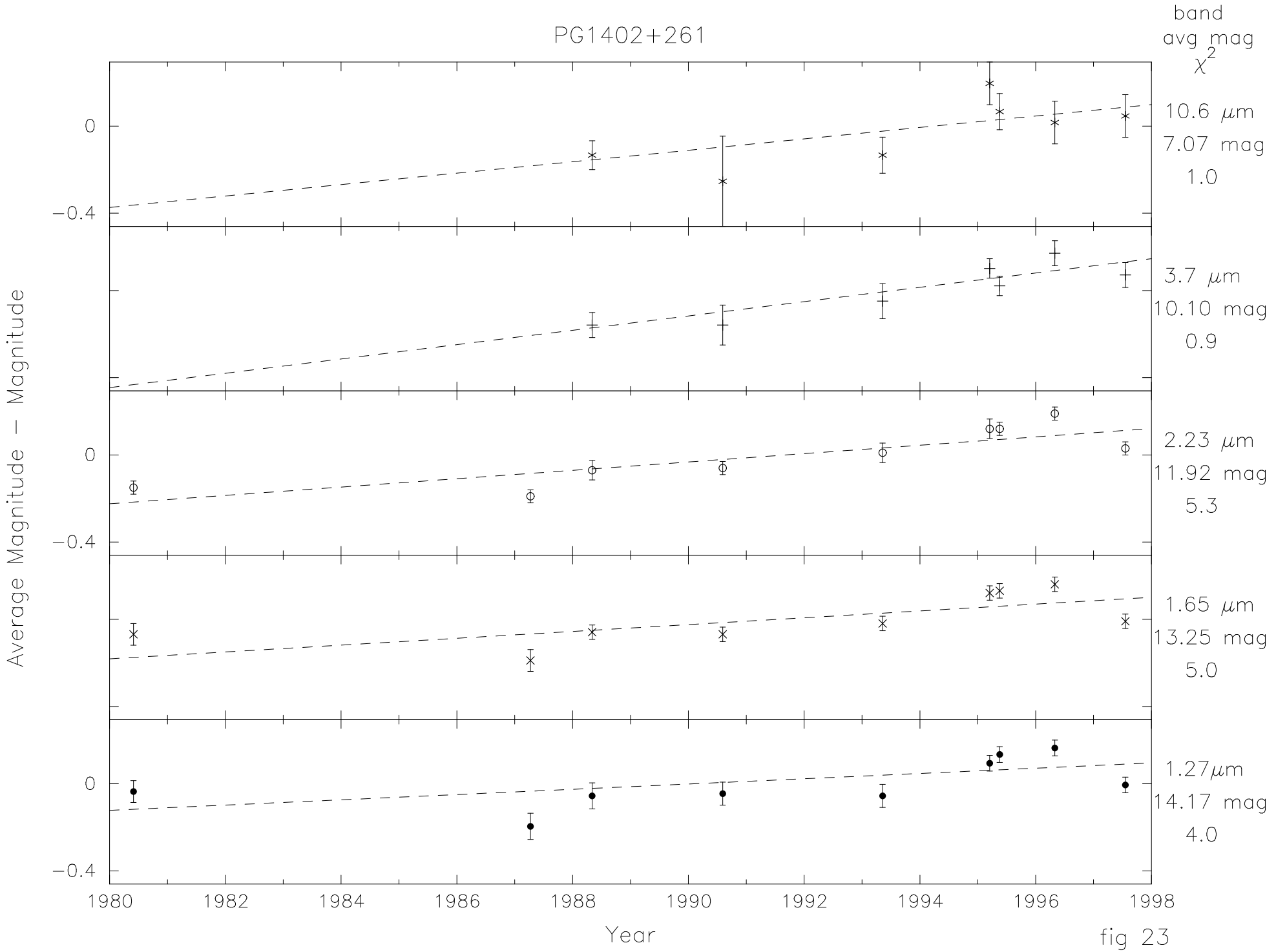
PG1402+261
band
avg mag
χ^2
10.6 μm
7.07 mag
1.0
3.7 μm
10.10 mag
0.9
2.23 μm
11.92 mag
5.3
1.65 μm
13.25 mag
5.0
1.27μm
14.17 mag
4.0
0
−0.4
Average Magnitude − Magnitude
1980
1982
1984
1986
1988
1990
1992
1994
1996
1998
Year

fig 23

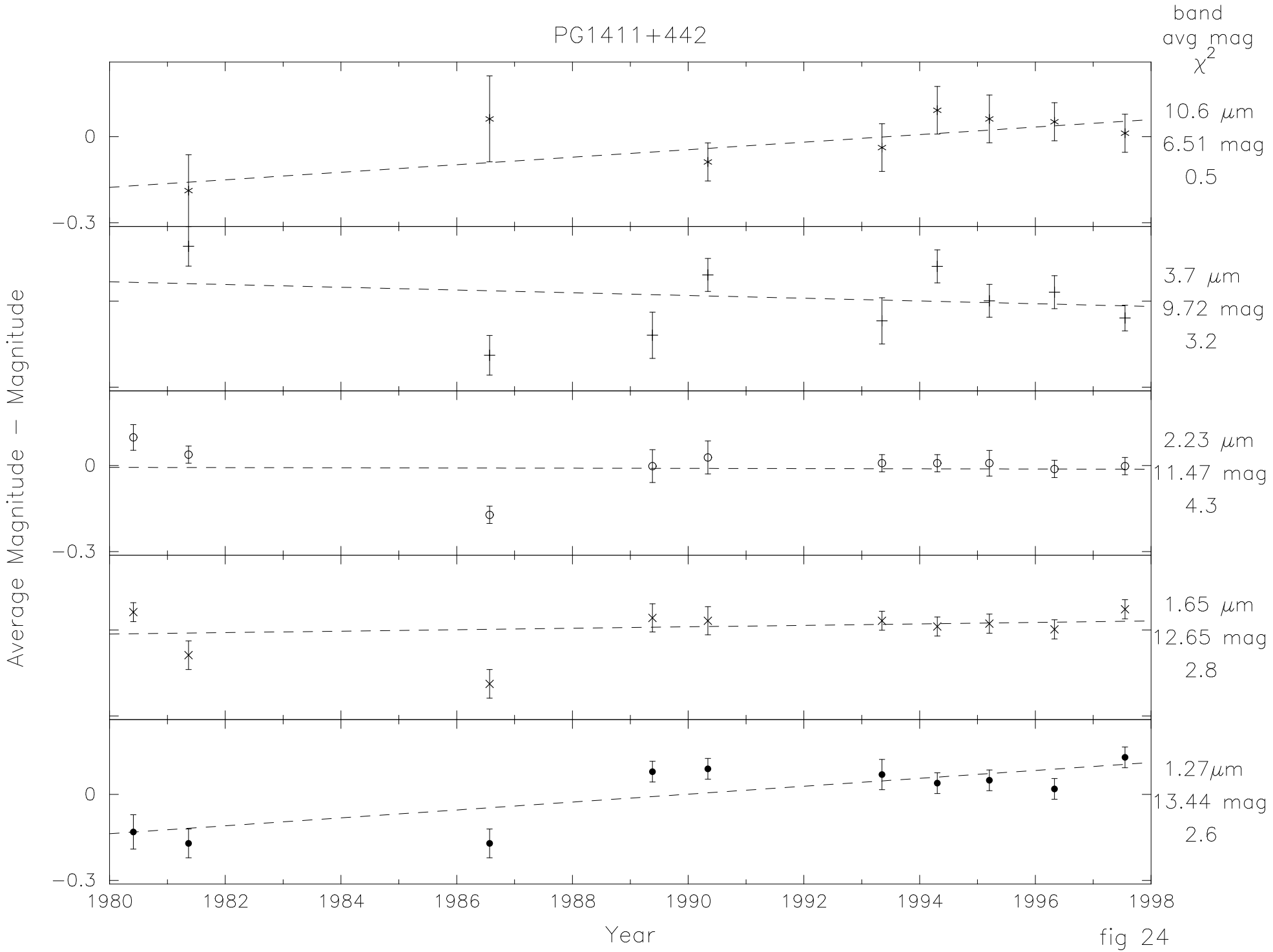
PG1411+442
band
avg mag
χ^2
10.6 μm
6.51 mag
0.5
3.7 μm
9.72 mag
3.2
2.23 μm
11.47 mag
4.3
1.65 μm
12.65 mag
2.8
1.27μm
13.44 mag
2.6
Average Magnitude − Magnitude
0
−0.3
1980
1982
1984
1986
1988
1990
1992
1994
1996
1998
Year

fig 24

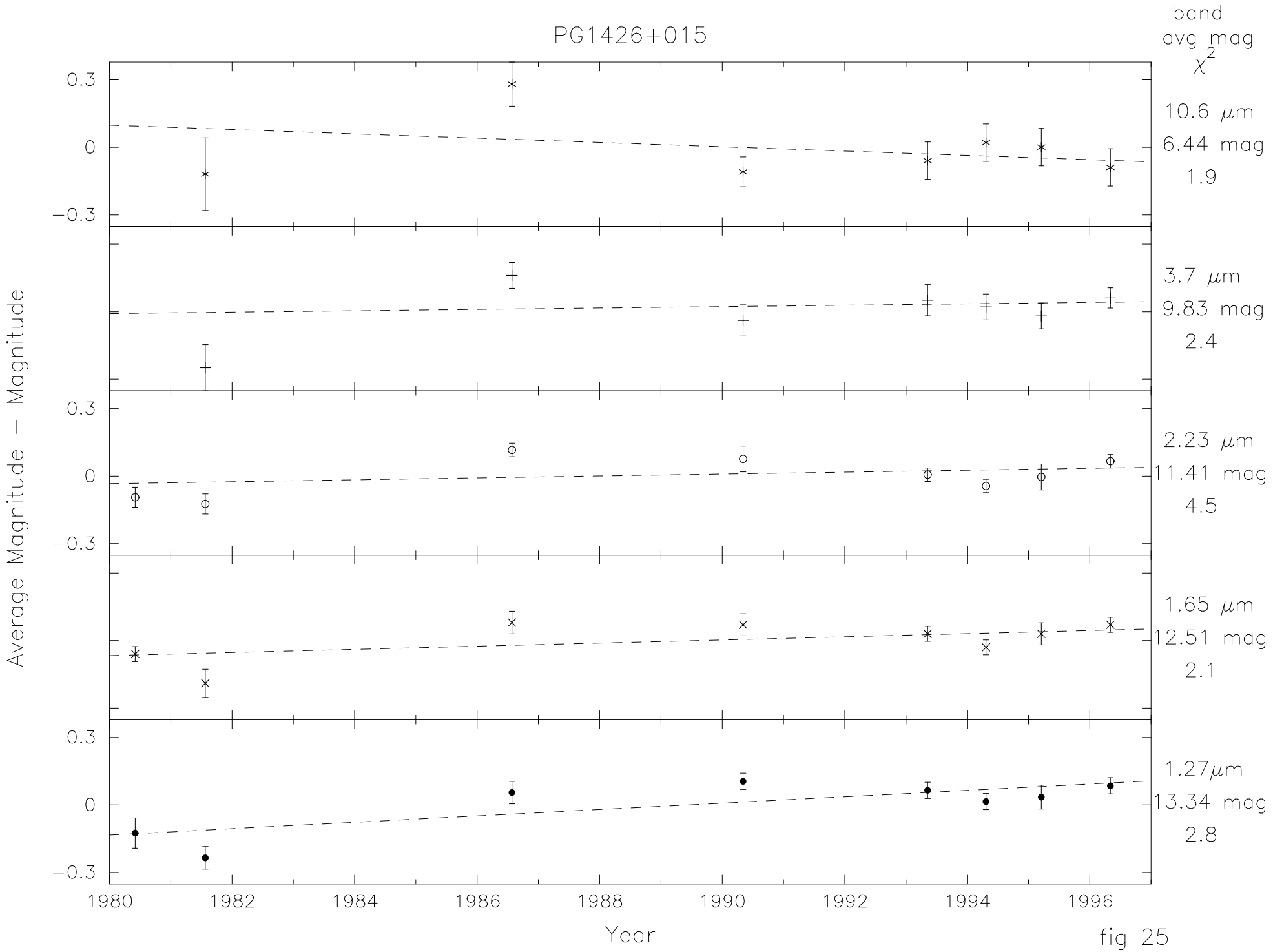
PG1426+015
band
avg mag
χ^2
10.6 μm
6.44 mag
1.9
3.7 μm
9.83 mag
2.4
2.23 μm
11.41 mag
4.5
1.65 μm
12.51 mag
2.1
1.27μm
13.34 mag
2.8
0.3
0
−0.3
1980
1982
1984
1986
1988
1990
1992
1994
1996
Year
Average Magnitude − Magnitude

fig 25

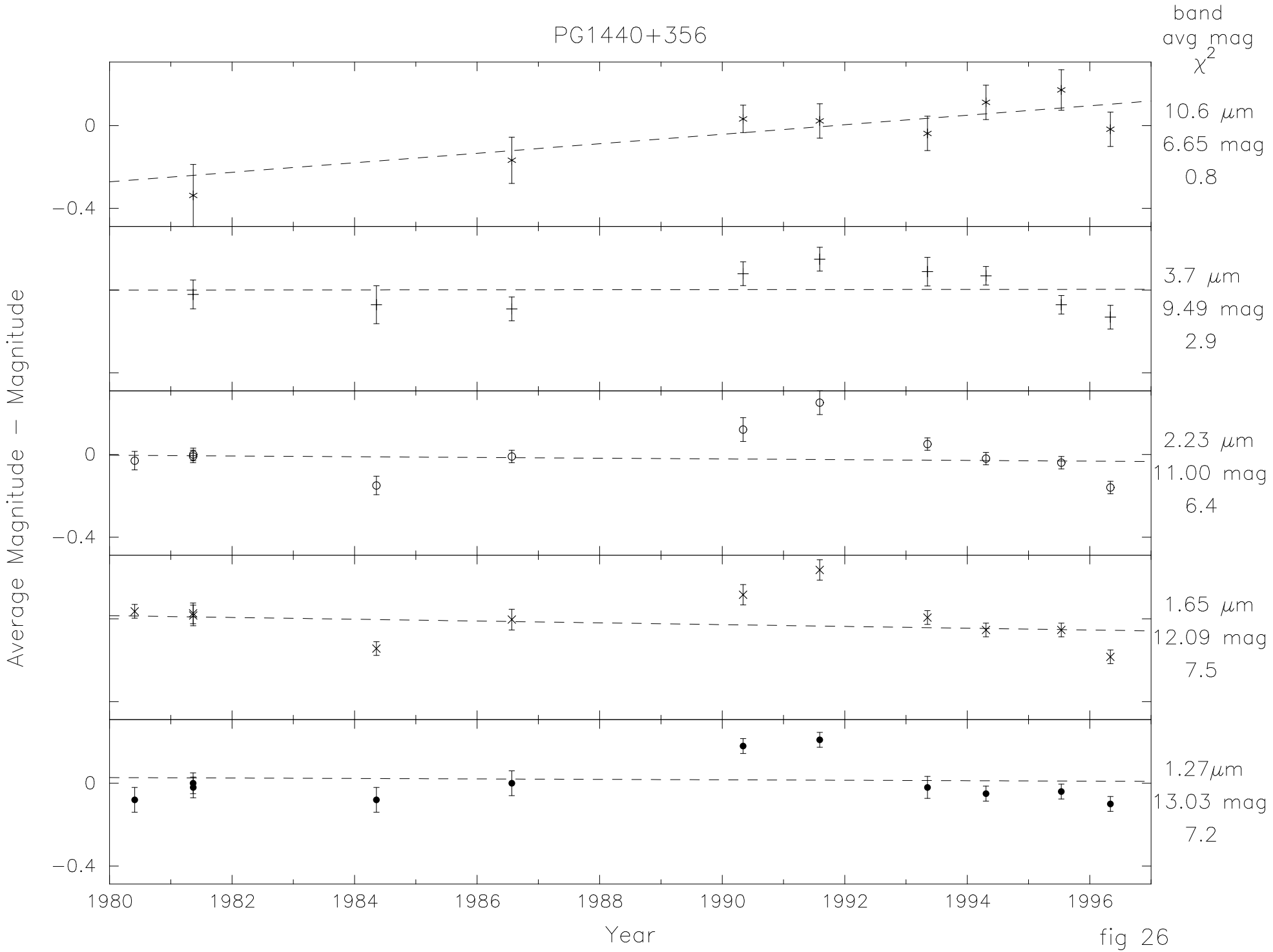
PG1440+356
band
avg mag
χ^2
10.6 μm
6.65 mag
0.8
3.7 μm
9.49 mag
2.9
2.23 μm
11.00 mag
6.4
1.65 μm
12.09 mag
7.5
1.27μm
13.03 mag
7.2
0
−0.4
Average Magnitude − Magnitude
1980
1982
1984
1986
1988
1990
1992
1994
1996
Year

fig 26

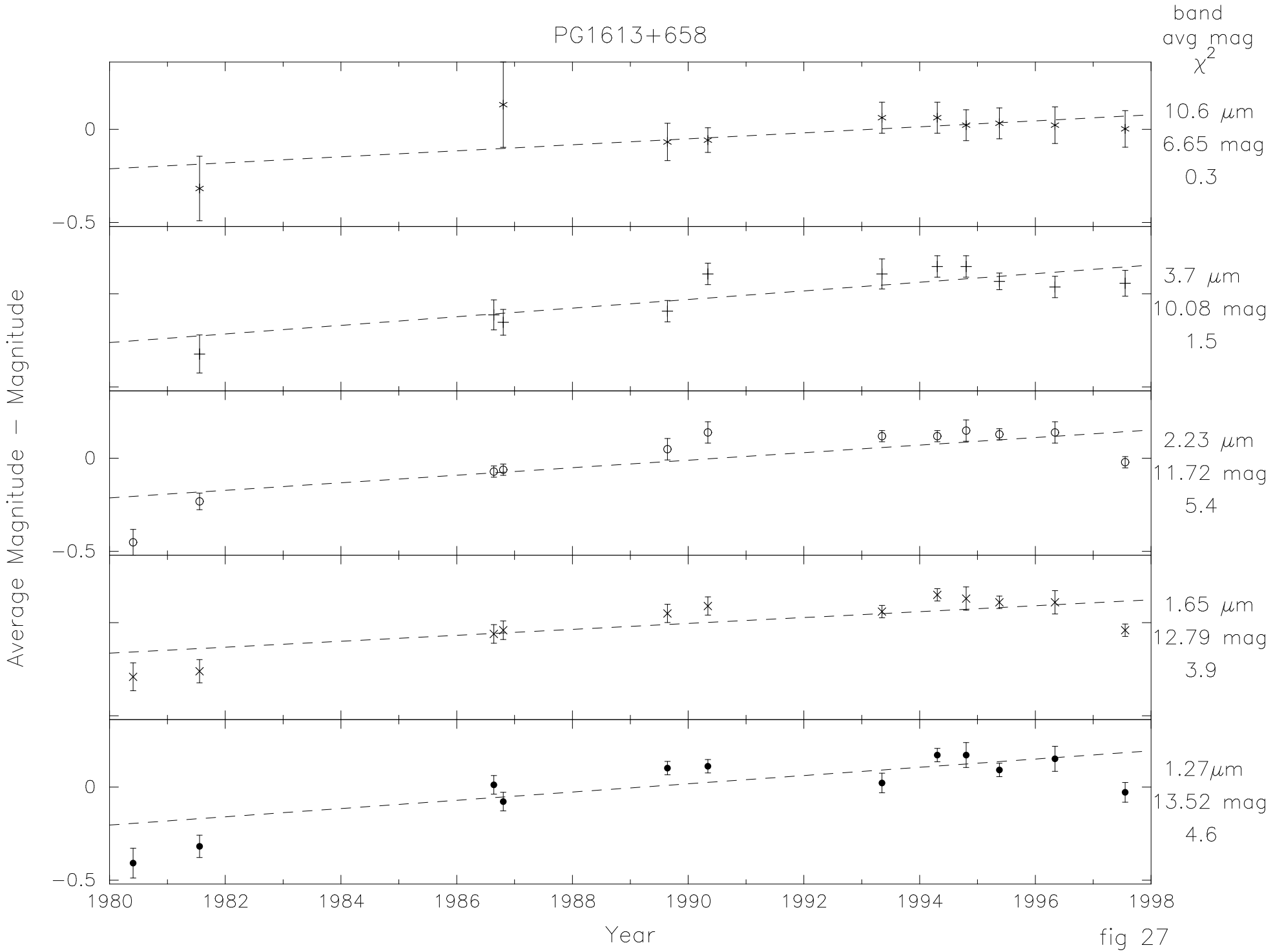
PG1613+658
band
avg mag
χ^2
10.6 μm
6.65 mag
0.3
3.7 μm
10.08 mag
1.5
2.23 μm
11.72 mag
5.4
1.65 μm
12.79 mag
3.9
1.27μm
13.52 mag
4.6
Average Magnitude − Magnitude
Year
0
−0.5
1980
1982
1984
1986
1988
1990
1992
1994
1996
1998

fig 27

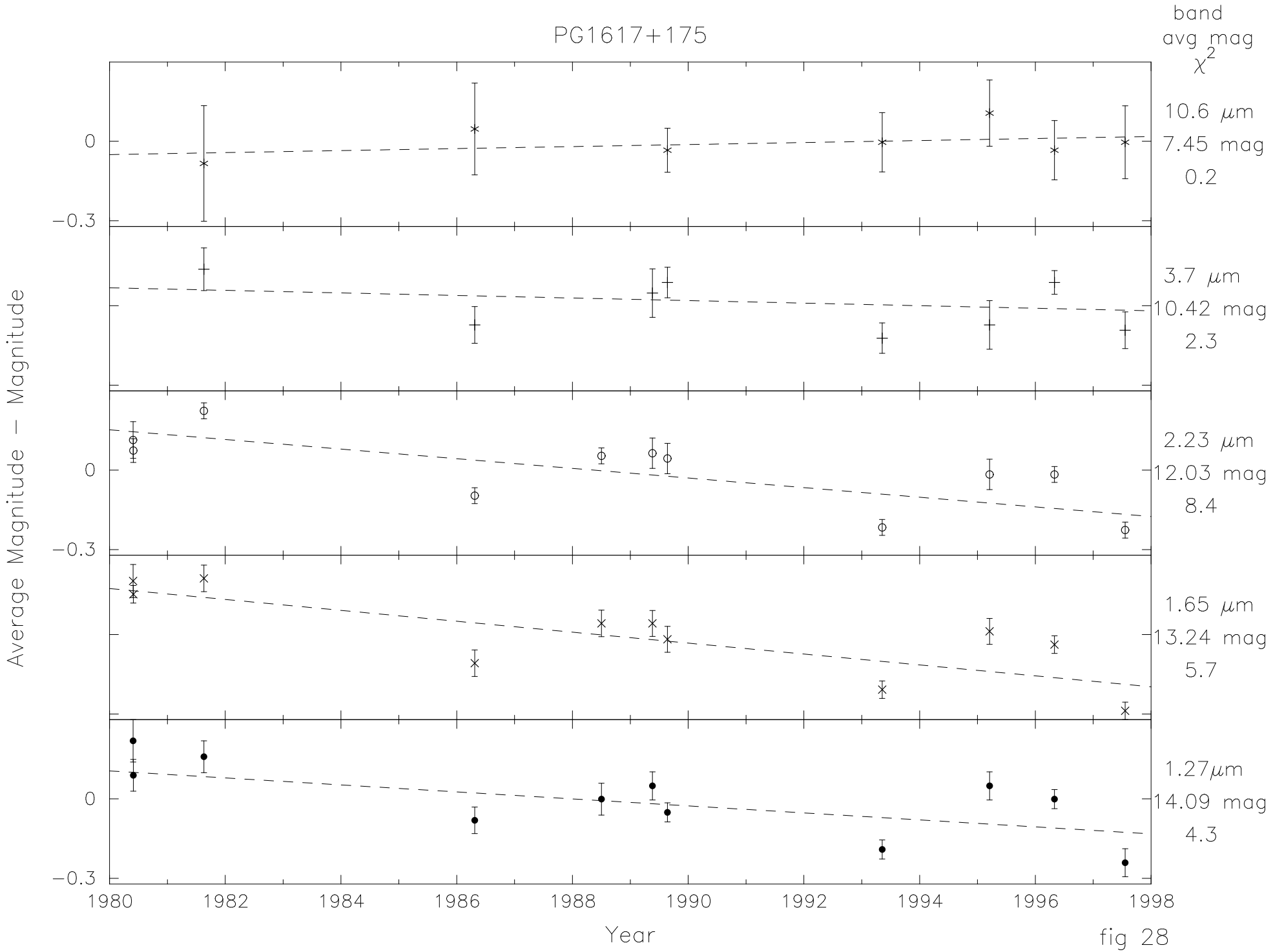
PG1617+175
band
avg mag
χ^2
10.6 μm
7.45 mag
0.2
3.7 μm
10.42 mag
2.3
2.23 μm
12.03 mag
8.4
1.65 μm
13.24 mag
5.7
1.27μm
14.09 mag
4.3
Average Magnitude − Magnitude
0
−0.3
1980
1982
1984
1986
1988
1990
1992
1994
1996
1998
Year

fig 28

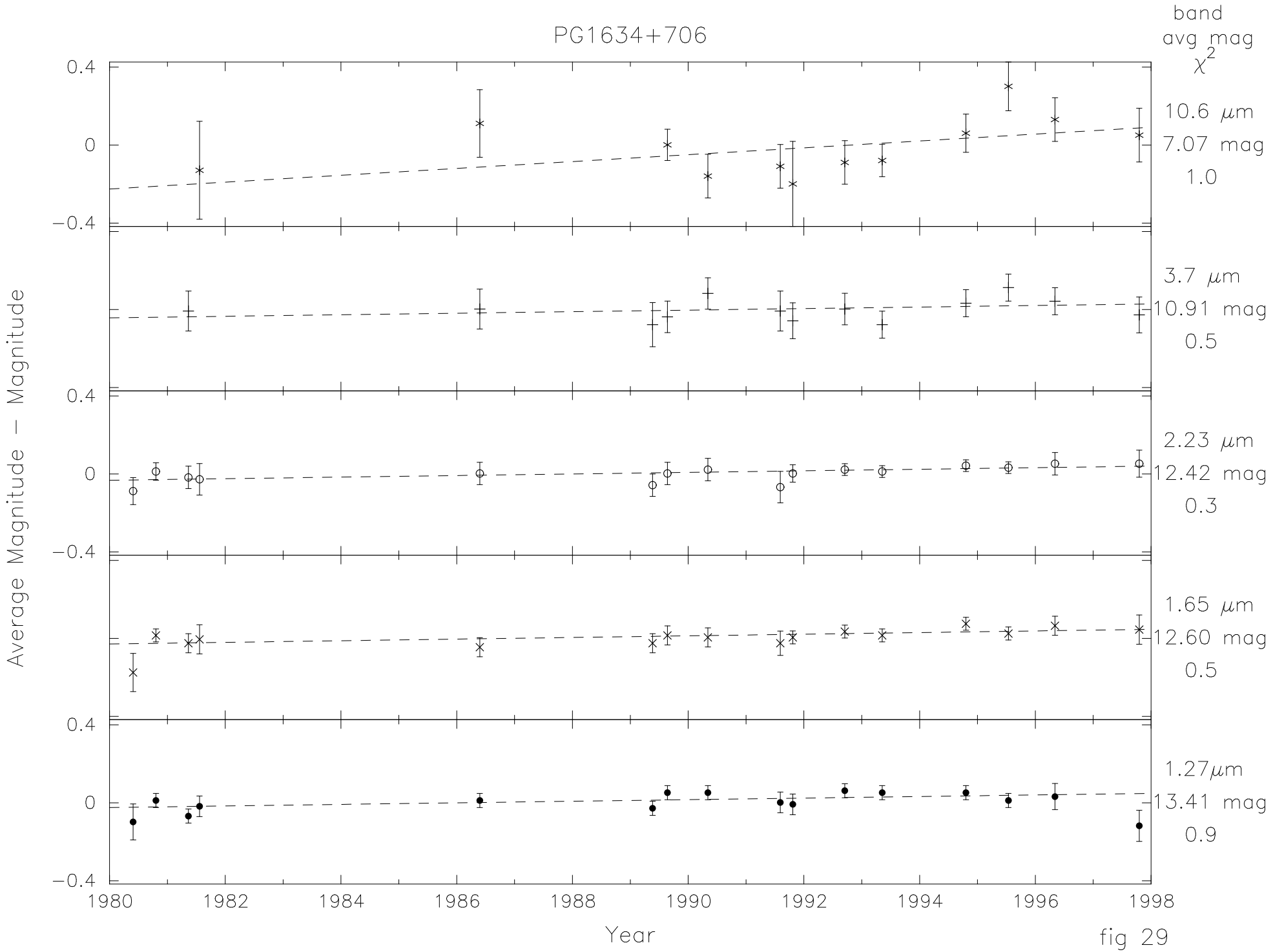
PG1634+706
band
avg mag
χ^2
10.6 μm
7.07 mag
1.0
3.7 μm
10.91 mag
0.5
2.23 μm
12.42 mag
0.3
1.65 μm
12.60 mag
0.5
1.27μm
13.41 mag
0.9
0.4
0
−0.4
1980
1982
1984
1986
1988
1990
1992
1994
1996
1998
Year
Average Magnitude − Magnitude

fig 29

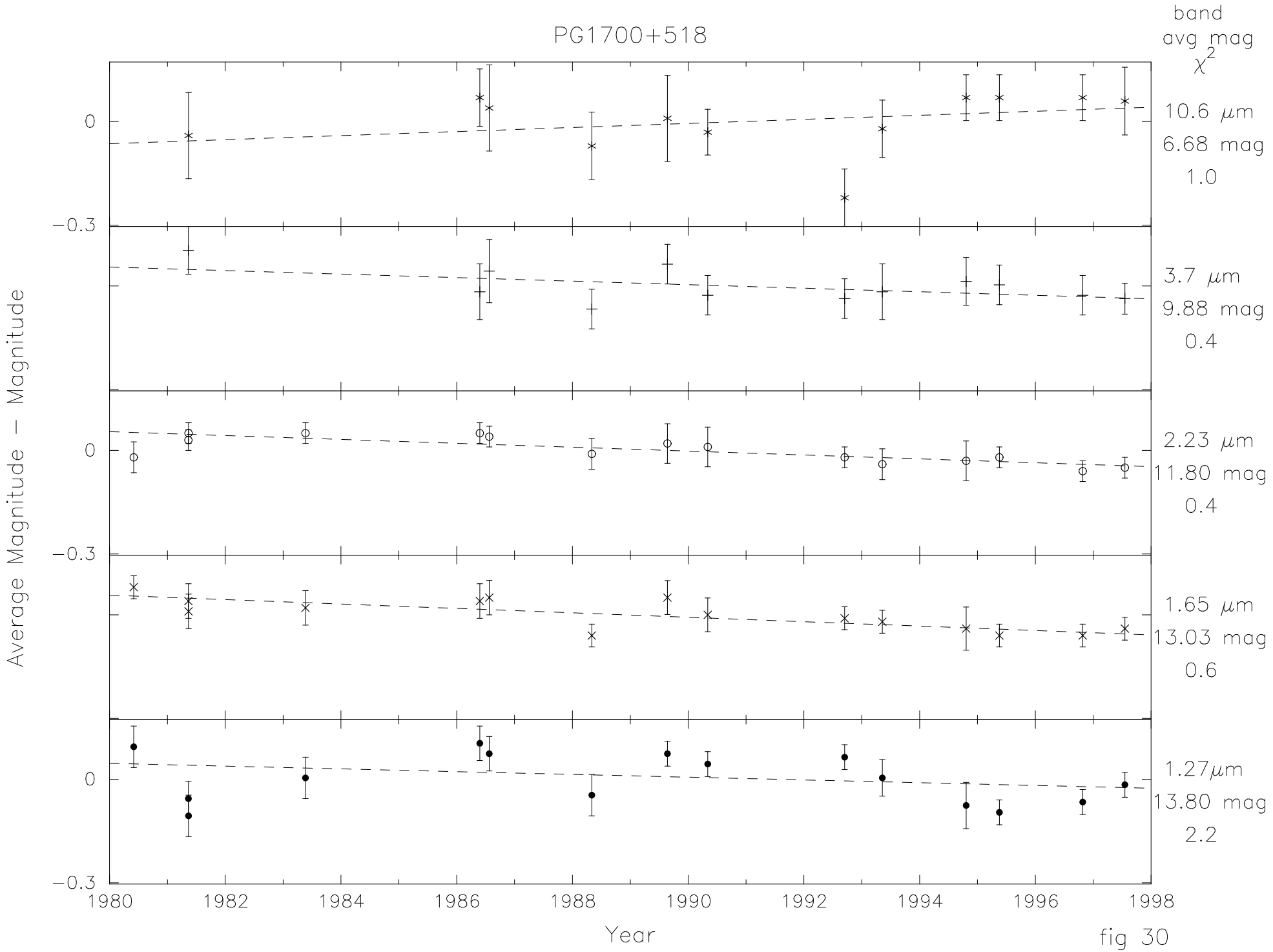
PG1700+518
band
avg mag
χ^2
10.6 μm
6.68 mag
1.0
3.7 μm
9.88 mag
0.4
2.23 μm
11.80 mag
0.4
1.65 μm
13.03 mag
0.6
1.27μm
13.80 mag
2.2
Average Magnitude − Magnitude
Year
0
−0.3
1980
1982
1984
1986
1988
1990
1992
1994
1996
1998

fig 30

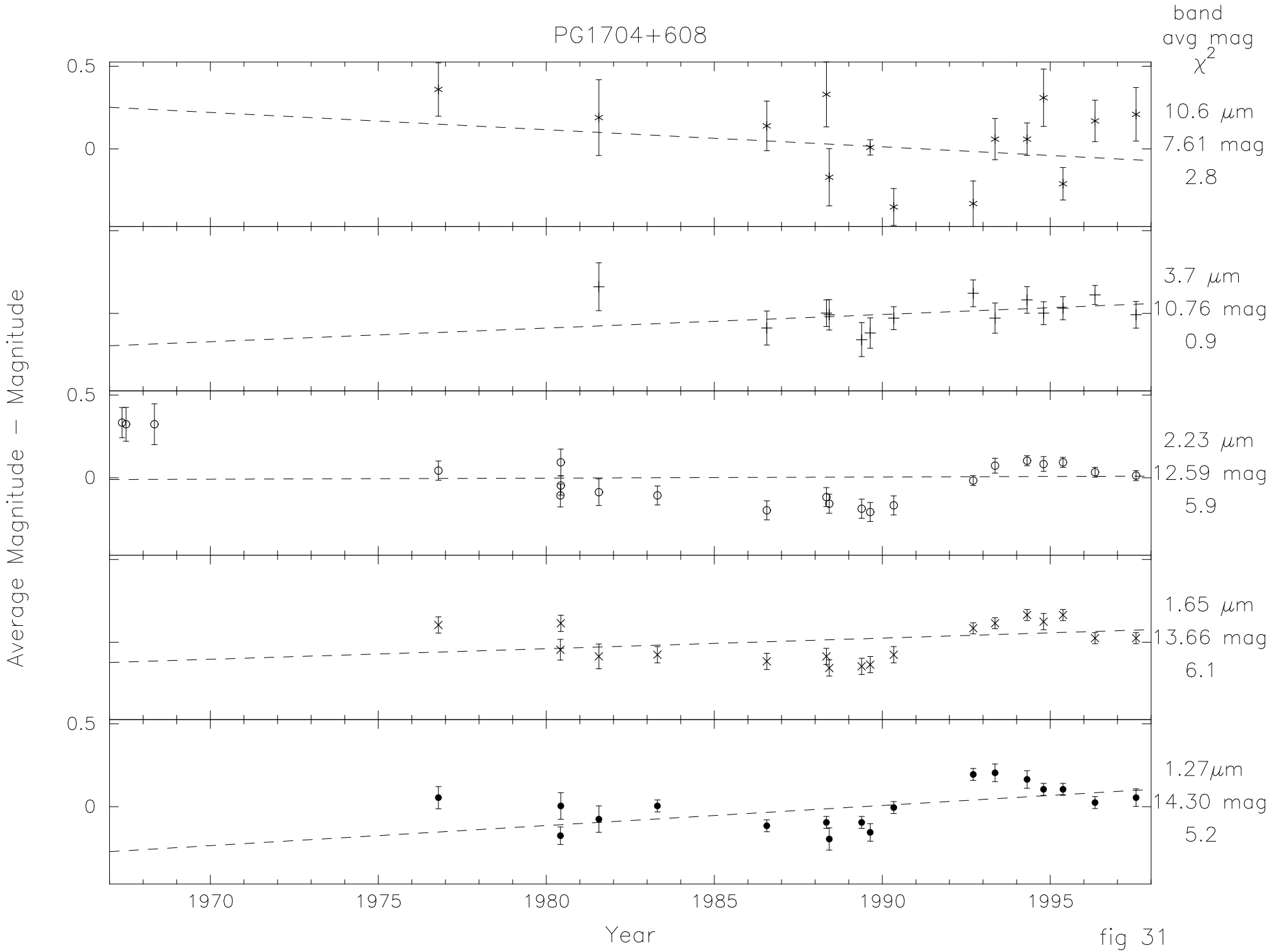
PG1704+608
band
avg mag
χ^2
10.6 μm
7.61 mag
2.8
3.7 μm
10.76 mag
0.9
2.23 μm
12.59 mag
5.9
1.65 μm
13.66 mag
6.1
1.27μm
14.30 mag
5.2
0.5
0
1970
1975
1980
1985
1990
1995
Year
Average Magnitude − Magnitude

fig 31

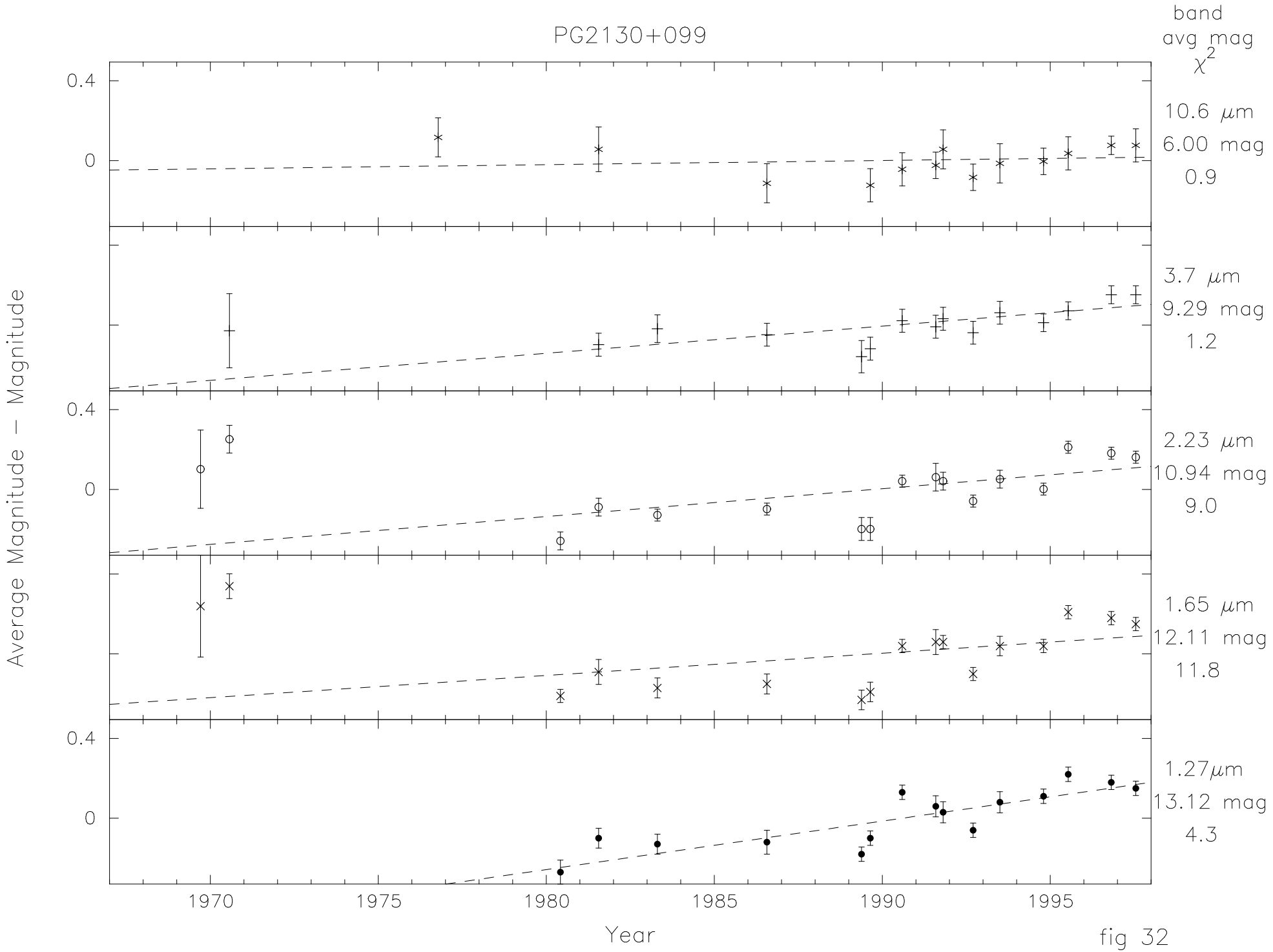
PG2130+099
band
avg mag
χ^2
10.6 μm
6.00 mag
0.9
3.7 μm
9.29 mag
1.2
2.23 μm
10.94 mag
9.0
1.65 μm
12.11 mag
11.8
1.27μm
13.12 mag
4.3
0.4
0
1970
1975
1980
1985
1990
1995
Year
Average Magnitude − Magnitude

fig 32

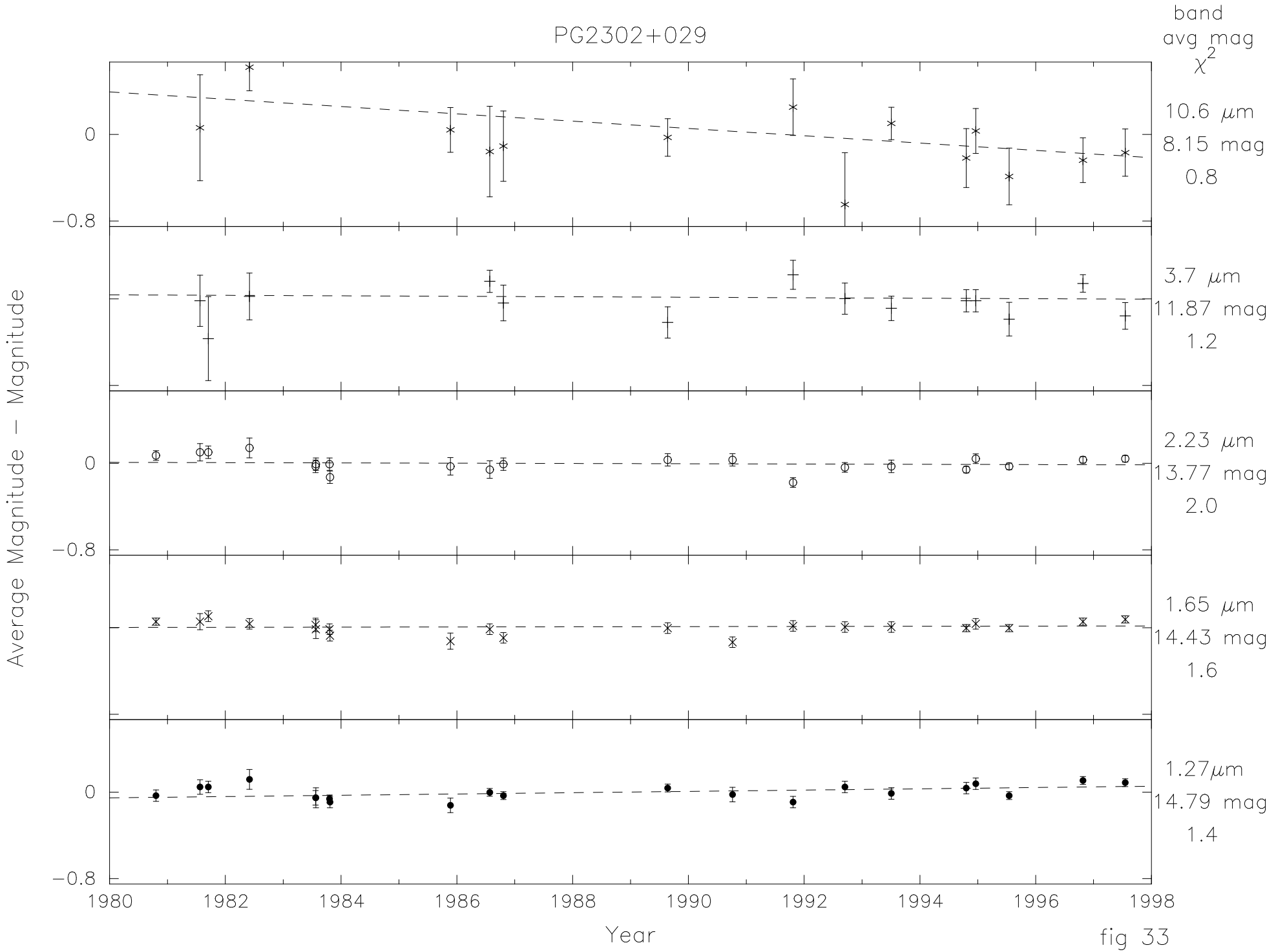
PG2302+029
band
avg mag
χ^2
10.6 μm
8.15 mag
0.8
3.7 μm
11.87 mag
1.2
2.23 μm
13.77 mag
2.0
1.65 μm
14.43 mag
1.6
1.27μm
14.79 mag
1.4
Average Magnitude − Magnitude
0
−0.8
1980
1982
1984
1986
1988
1990
1992
1994
1996
1998
Year

fig 33

Variability of Quasars at 10 μm

G. Neugebauer

and

K. Matthews

Palomar Observatory, California Institute of Technology, 320-47, Pasadena, CA 91125

Electronic mail: gxn@caltech.edu, kym@caltech.edu

Received _____; accepted _____

ABSTRACT

Twenty five low redshift quasars have been monitored for several decades at five near- and mid-infrared wavelengths to detect rapid variations which would indicate that a nonthermal component was present in the "10 μm bump". Such variability has apparently been detected in several radio loud quasars and in the radio quiet quasar PG1535+547. In addition, the structure function of PG1226+023 shows that an apparently periodic component is present in its near-infrared emission.

Subject headings: quasars, infrared, variability

1. Introduction

The presence of a local maximum in the continuum spectral energy distribution of quasars at rest wavelengths around 10 μm has been well established (see, e.g., Sanders et al. 1989; Elvis et al. 1994). The maximum is ubiquitous in both radio loud and radio quiet quasars, and the two types of quasars cannot be distinguished from each other on the basis of their infrared properties. The mechanism responsible for the emission in the "bump" has been the subject of debate (see e.g., Bregman 1994; Ulrich, Maraschi & Urry 1997) although the ultimate source of the luminosity is generally assumed to be the release of gravitational energy by matter in an accretion disk falling into a black hole. Both nonthermal emission from the nucleus and thermal emission from heated dust is assumed to contribute to the infrared emission in most quasars, but the infrared emission in radio loud quasars has generally been taken to be dominated by nonthermal emission (see e.g., Robson et al. 1993; Bloom et al. 1994 and references therein). On the other hand, the evidence is strong that thermal emission from heated dust dominates the emission of radio quiet quasars (see the discussion and references in e.g., Sanders et al.; Bregman). In particular, the spectral energy distribution around 1 μm exhibits an almost universal minimum which is most naturally explained by the sublimation of dust grains at temperatures of about 2,000 K. There is also a drop in the continuum at submillimeter wavelengths which again is naturally explained by a drop in the opacity of dust grains with increasing wavelength.

As pointed out by Sanders et al. (1989), synchrotron models for the emission from quasars require brightness temperatures exceeding $m_e c^2/k \approx 10^{10}$ K or about 10^8 times larger than the brightness temperatures which characterize thermal emission. Consequently the emitting region, if the emission at 10 μm is thermal, will be $\approx$10,000 times larger than that of a nonthermal source, and therefore the detection of a small source would eventually be able to settle unambiguously whether nonthermal emission was present. The predicted

angular sizes even from thermally emitting grains around quasars are, however, typically much smaller than $0.1''$ and such small sizes cannot be measured directly at the present time (see e.g., Sanders et al.).

The extreme size difference implies that a way to discriminate between the two mechanisms is to look for variability in the mid-infrared emission. If the emission varies on short time scales, causality argues that the size of the emitting region is small and thus that the emission is nonthermal. As discussed below, for a central source with a typical quasar luminosity, grains which dominate the thermal emission at the mid-infrared wavelengths are located tens to hundreds of light years from the nucleus and so significant variability on a time scale shorter than decades would rule out thermal models. Note, however, that a lack of variability is not sufficient to rule out nonthermal models.

In this paper we present observations of 25 quasars at 10.6 μm intended to distinguish between thermal and nonthermal emission in the 10 μm bump. The 10.6 μm atmospheric window was chosen as the longest wavelength at which to conveniently make routine measurements from a ground based site. Measurements at the mid-infrared wavelengths such as 10.6 μm or longer are necessary since, even if the radiation is thermal emission from heated dust, the shorter infrared wavelengths sample hotter grains closer to the nucleus and short term variations of their thermal re-radiation can exist as a direct result of the variable nonthermal emission from the nucleus. The Hubble constant will be taken to be H_0=75 km s^{-1} Mpc^{-1} unless otherwise specifically stated.

Observations were also made at wavelengths in the near-infrared atmospheric windows in order to support the 10.6 μm measurements. These observations proved interesting in their own right and thus a preliminary analysis of these data is included in this paper.

2. Sample

Twenty five quasars from the list of optically selected quasars of the Palomar Bright Quasar Survey (Schmidt & Green 1983) were monitored for variability in the near-infrared and are tabulated in Table 1. The sample was made up of quasars in the Palomar Bright Quasar Survey which had been established to be bright at 10.6 μm from measurements made by the Caltech group (Neugebauer et al. 1987). The selection was in no way systematic or exhaustive; any other bias in the selection has not been established.

Twenty of the quasars in the sample were detected by IRAS at 60 μm and most of these quasars were seen in all of the IRAS bands (Sanders et al. 1989). Exceptions are PG1535+547 which was detected by IRAS only at 12 and 25 μm, not at 60 and 100 μm, and the quasars PG0026+129, PG1617+175 and PG2302+029 which were not detected in any of the IRAS bands. PG2209+184 is in a location which was not scanned by the IRAS satellite.

The spectral energy distributions from 0.3 nm to 6 cm are shown in Sanders et al. (1989) while the spectral energy distributions of thirteen quasars of the sample from 10 keV x-rays to radio wavelengths are given by Elvis et al. (1994). Wilkes et al. (1998) include the quasar PG1351+640 in their study of ISO data of the far-infrared continuum of quasars.

Bolometric luminosities, which represent the estimated luminosity of the quasars from 10^{12} to 10^{17} Hz, are taken from Sanders et al. (1989). They are included in Table 1 and their distribution is shown in Figure 1; the median bolometric luminosity is L_{bol}=1.6×$10^{12}L_{\odot}$. Schmidt & Green (1983) have designated five of the objects in the sample (PG0007+106, PG1119+120, PG1501+106, PG1535+547 and PG2209+184) as "Seyfert I nuclei or low-luminosity quasars" based on their having absolute B magnitudes M_B > -23.0 mag with H_0=50 km s^{-1} Mpc^{-1}. The redshifts of quasars in the sample are also taken from

Sanders et al. and given in Table 1. The distribution of redshifts is included in Figure 1; the median redshift is z=0.089. The mean 10.6 μm magnitudes obtained in this study range from 8>$[10.6]_{avg}$ >5 mag.

Twenty of the quasars are radio quiet while five are radio loud; see Table 1. The classification as either radio loud or radio quiet is that given by Sanders et al. (1989). The separation between the two types has been made at $\log[\nu f_\nu(6\text{ cm})/\nu f_\nu(1\ \mu\text{m})] = -4$ using the radio data of Kellermann et al. (1994). The distinction between radio loud and radio quiet is open to discussion. For example, Kukula et al. (1998) have called PG0007+106, which Sanders et al. classify as radio loud, a "radio-intermediate quasar". Becker (1998, private communication) has argued that modern complete surveys at radio frequencies show there is a continuun between radio loud and radio quiet quasars.

3. Observations

Caltech measurements of selected quasars at 10.6 μm were obtained from 1974 to the 1998. Systematic monitoring observations specifically to measure variability at 10.6 μm were started in 1988. The observations after that time were made at the Cassegrain f/70 focus of the 200-inch Telescope at Palomar Mountain using beams with 5″ diameters. Measurements were made in the J, H, K, L', and N photometric bands; the central wavelengths and half power wavelength widths of the filters used are given in Table 2. A single element Ge:Ga bolometer at pumped liquid helium temperature was used to measure the flux at 10.6 μm and a single element InSb photovoltaic detector at solid nitrogen temperature was used to observe wavelengths between 1.27 and 3.7 μm. The effects of the sky emission were suppressed by chopping the beam in a north-south direction with the f/70 secondary mirror at either 5 or 50 Hz and nodding the telescope, also in a north-south direction, by either 15″ (1.27-3.7 μm) or 6″ (10.6 μm). The telescope tracking was maintained by using an

offset guider with a visual guide star.

For completeness, compatible observations made before 1988 are incorporated into the data-base of this study. A few of these were made at the 100-inch Hooker Telescope at Mt. Wilson. During the total time span, the instrumentation evolved gradually. The bolometer system for the 10.6 μm observations has, however, remained intact since 1973 and the same filters have been used in various near-infrared InSb systems which were introduced in 1972, 1975, 1981 and 1982. Care was taken to ensure that the photometric results were consistent during all the changes.

In the decade following 1988, the majority of the 25 quasars in the sample were sampled once per year, but for a few objects the time interval between observations sometimes exceeded three years; all 25 quasars have measurements made at all five wavelengths on at least seven nights. Observations at the four shorter wavelengths typically took a total of 20 minutes and those at 10.6 μm typically took 40 minutes. Observations were generally made when the quasars were at $\lesssim$1.7 air masses and standard air mass corrections were applied. Only observations made on photometrically clear nights when the full width at half maximum (FWHM) of the visual image was $\lesssim 2''$ were included in the final data set. In total there were some 1,900 photometric measurements of quasars included.

The quasar observations were accompanied by a comparable number of measurements of "standard" stars to maintain photometric accuracy. In the four shorter wavelength bands, the stars identified by Elias et al. (1982) were used. At 10.6 μm, stars previously measured by the Caltech group and tabulated in Table 3 were utilized. The integrity of the photometric standards was checked by the internal consistency of the photometric sensitivity of several measurements made on the same night and throughout this study. The (population) standard deviation of the sensitivity measured on any one night for the three shortest bands was typically 0.02 mag; that of the 3.7 μm-band was 0.04 mag and that of

the 10.6 μm-band was 0.05 mag. The standard deviations of the absolute sensitivities of the system in the different wavelength bands, i.e. the sensitivity which would have been assumed if no "standard" stars were measured, were $\sim$0.1 mag including one period during 1991-1992 when the sensitivity of the different wavelength bands differed by as much as $\sim$0.5 mag. The sense of the dispersion in these sensitivities was completely consistent with effects of the mirror coating and from the eruption of Mt. Pinatubo.

The uncertainties in the magnitudes were calculated as the square root of the quadratic sum of the statistical uncertainty in the object plus the dispersion in the "standards" plus an uncertainty which is representative of the systematic uncertainty in making the observation. The later was somewhat arbitrarily assigned the value 0.02 mag, based on experience with similar measurements of objects with large signal to noise ratios. Generally the statistical uncertainties dominated the 10.6 μm observations; systematic uncertainties often dominated the 1.27 to 2.23 μm observations.

4. Results

Four representative data sets are shown in Figures 2–5; they will be discussed in detail below. The data of the remaining 21 quasars in the sample are given in Figures 13–33 in the Appendix. All these figures are similar in that they include observations in the five wavelength bands presented in the same order from bottom to top. Unless specifically indicated, the ordinates of each figure are scaled to be the same for all wavelength bands for that object; the scales were set to include the largest excursions measured in any band for that object. Some observations made before 1989 have previously been published by Neugebauer et al. (1989).

A measure of the variability relative to the uncertainties in the measurements for each

wavelength band is provided by the reduced chi-square:

$$\chi^2 \equiv \frac{1}{N} \times \sum_{i=1}^{N} \frac{(m_i - <m>)^2}{\delta m_i^2}$$

where m_i is the magnitude observed on a specific date and wavelength, $< m >$ is the magnitude of the observations at that wavelength as determined by a linear fit to all the measurements at that wavelength throughout the study, N is the number of observations and δm_i is the uncertainty in the measurement of m_i. As discussed below, a long term drift in a nonthermal component can be transferred to a thermal component. The reduced χ^2 for each of the 25 objects in the sample for each wavelength is included in Figures 2–5 and 13–33. A limit on the inherent variability necessary to produce large values of chi-square at 10.6 μm was set by the typical uncertainty of 0.1 mag, or 10% at that wavelength. This contrasts to the shorter wavelengths where uncertainties of a few percent were routinely achieved. Nonetheless, of four of the five radio loud quasars observed, all but PG1211+143, and six of the 15 radio quiet quasars had reduced $\chi^2 > 1.5$ at 10.6 μm indicating measurable variability. At 2.23 μm, the flux variations from all the radio loud quasars and all but two radio quiet quasars exceeded this limit. In fact, as discussed below, the median variability of the majority of the sample exceeded 0.1 mag at all wavelengths. Thus, we conclude that we have measured variability, certainly at the shorter wavelengths, but also at 10.6 μm, in some of the quasars of this sample.

It is also possible to calculate reduced χ^2 by converting each magnitude to a flux density, a linear quantity, finding the average flux density, and then calculating the reduced χ^2. Although the reduced χ^2 found in this manner differs slightly from that found from the magnitudes because of the transformation of the uncertainties, the two formulations give qualitatively the same results. The χ^2 derived from the magnitudes and presented with the figures are generally smaller than those derived using the flux densities.

In some cases, even where the reduced χ^2 is consistent with a constant slope, there is apparently often a low frequency variation present with a period of about a decade which appears as a correlated variation at more than one wavelength. A different way of presenting the results, which emphasizes possible correlations in the magnitudes at the cost of time knowledge, is to compare the photometric changes of an object that was measured at the same two wavelengths on two nights. In the following, all possible comparisons, i.e., differences between all nights when the same two wavelengths were observed, are included. Examples which illustrate apparent correlated changes at all wavelengths are shown in Figure 6 (PG1226+023, radio loud) and Figure 7 (PG1535+547, radio quiet) while Figure 8 gives an example of both corellated and un-correlated changes (PG1351+640, radio loud). Similar plots show that the changes at 1.27, 1.65 and 2.23 μm for all the quasars but PG1700+518 are apparently correlated. On the other hand, two thirds of the sample showed variations at 3.7 and 10.6 μm which are probably not correlated as evidenced by a probability of the null hypothesis of no correlation in excess of 0.10; undoubtedly, this is partially the result of the larger uncertainties at these wavelengths.

5. Discussion

5.1. Thermal model

In order to make a comparison with the observed results, a simple model of thermal re-radiation from heated grains was constructed. Dust grains were assumed to exist in concentric shells with a range of radii around a central luminosity source. The temperature of the grains at each radius was set by radiation balance between the photons absorbed from the central source and re-emitted by the grains. Silicate, graphite and blackbody grains were tried. The aggregate of the grains was assumed to be optically thin. The maximum grain temperature allowed before the grains were assumed to sublime was 2,000 K for graphite

grains and 1,500 K for silicate grains. The minimum temperature was arbitrarily assumed to be 100 K; the results were insensitive to these choices. Planck averaged emissivities were taken from Draine & Lee (1984) and the grain size distribution was taken to be that given by Mathis, Rumpl & Nordsieck (1977). The grain number density with size was assumed to have a power law dependence on radius; an inverse square dependence was most often used.

If the thermal model applies, if the grains are silicates and if the central bolometric luminosity is the median bolometric luminosity of the sample, L_{bol}=1.6×10$^{12}L_{\odot}$, the shell which contributes the maximum 10.6 μm signal has a diameter of about 55 light years. Half the flux observed in the 10.6 μm band would be emitted by grains located in shells with radii between 15 and 60 light years. In contrast, if the bolometric luminosity of the central source is only 2.8×10$^{11}L_{\odot}$, that of PG1535+547 the least luminous quasar in the sample, in this simplified model the shell which contributes the maximum 10.6 μm signal has a radius of only about 20 light years.

In order to characterize the response in thermal emission to variations in the nonthermal central source, a step increase in luminosity of the central source was assumed. The grains were assumed to respond instantly to the absorbed energy upon arrival of the photons from the central source. Typical responses predicted to be observed at 2.23, 3.7 and 10.6 μm if the grains were silicates are shown in the top of Figure 9 for a step amplitude in the central source from 1.4 × 10^{12} to 1.8×10$^{12}L_{\odot}$. As expected, the observed increase at 2.23 μm is predicted to be significantly faster than that at 10.6 μm since the grains responsible for the short wavelength radiation are hotter and hence closer to the central source. Although Figure 9 (top) illustrates the results of the model only for silicate grains, the amplitude of the response at 10.6 μm to a step change in the central luminosity is about one-third that at 2.23 μm over a wide range in luminosities and for graphite as well as silicate grains.

It is difficult from the presentation of Figure 9 to visualize the time it takes for the

grains in the envelope to respond to a change in the central luminosity. This time can conveniently be characterized by the time it takes the observed flux to go from 10 to 90% of its predicted final level if the central luminosity source has a step increase in luminosity. This 10 – 90% rise time is insensitive to the step amplitude, but depends strongly on the average luminosity of the central source. Figure 9 (bottom) shows the 10 – 90% rise times expected in observations at 2.23, 3.7 and 10.6 μm if the central luminosity source increases by 25%.

5.2. Specific examples

Figure 2 shows the most extensive set of observations obtained, those of PG1226+023 (3C273), a bright radio loud quasar with a flat radio spectrum. Variability at 10 μm accompanying variations over a wide range of wavelengths has previously been reported in this quasar by Rieke & Lebofsky (1979), Robson et al. (1983), Cutri et al. (1985), and Courvoisier et al. (1988). As discussed in these references, the nonthermal component is apparently sufficiently strong relative to the thermal component to be evident at all the infrared wavelengths. Indeed, the present observations confirm variability in PG1226+023 at all five of the near-infrared and mid-infrared wavelengths including 10 μm. PG1226+023 is one of two quasars included in both this sample and in the study by Smith et al. (1993), in the Johnson B band, of a large sample of radio loud quasars. This study showed apparently random vaiations in the visual flux with a peak-to-peak amplitude of about 0.5 mag.

Figure 3 shows observations of PG2209+184, another radio loud quasar with a flat radio spectrum; it is conjectured that the effects of a non-varying host galaxy masks the variations at wavelengths from 1.27 to 2.23 μm. Host galaxies have been observed associated with low redshift quasars by a large number of authors; see e.g. Bahcall et al. (1997) and

references therein. They have been observed in the near-infrared by, among others, McLeod & Rieke (1994a, 1994b); recent near-infrared HST obsevations of host galaxies are presented by Hines et al (1999; private communications). Near-infrared images of 15 of the quasars in this sample that dilineate the host galaxies have been obtained in an accompanying observing program. The median contribution of the putative host galaxy above that of a point like source between the seeing disk of $<1''$ diameter and an outer diameter of $5''$ (the beam diameter used in this study) is about 10% of the 1.65 μm flux of the quasar. Of those imaged, PG2209+184 has the largest host contribution to the observed flux; at 1.65 μm about one quarter of the quasar flux in a $5''$ diameter beam can be attributed to a host galaxy. The hosts are thought to be normal galaxies (see e.g., Neugebauer, Matthews & Armus 1995) so their contribution to the 10.6 μm, and probably 3.7 μm, flux is negligible, although the presence of a host galaxy serves to damp out 2.23 μm and shorter wavelength variations. The detailed nature of the hosts will be discussed in a future publication, but for the purposes of this paper, their effect can be ignored at 3.7 and 10.6 μm.

The observations of PG1501+106, a radio quiet quasar, provide a data set (Figure 4) where the 10.6 μm variability is markedly less than, and uncorrelated with, that at the shorter wavelengths. Presumably this is a case where the 10.6 μm emission is dominated by thermal emission from dust grains with subsequently smaller variations at 10.6 μm than at the shorter wavelengths. Specifically, the smooth rise at 10.6 μm is consistent with the model described above if there were a long period increase in the nonthermal near-infrared source in the decade before these observations were made.

In contrast to the previous example, PG1535+547, another radio quiet quasar, shows apparent variability at all measured wavelengths as illustrated in Figure 5. Although the variation at 10.6 μm has a reduced χ^2 consistent with a constant flux (reduced $\chi^2 = 1.27$), the deviations at all of the wavelengths are apparently correlated (Figure 7) and thus

convince us that true variations on a time scale as short as decades is being observed at 10.6 μm. At first sight, the data in Figure 5 indicate that, in this quasar at least, nonthermal processes play a significant part in producing the 10.6 μm bump. It should be noted that PG1535+547 is the least luminous of the quasars in the sample. Still, the short time of the variations would require a special composition of the grains if the radiation were purely thermal. The amplitude of the 10.6 μm observations in relation to the variations in the near-infrared is also inconsistent with the simple model of thermal emission. Neither a thermal or nonthermal model easily explains the apparent phase advance at 3.7 μm.

5.3. Median Variability

Netzer et al. (1996) have monitored 44 radio loud quasars at B and R for a period of six years with a mean sampling of four to six times per year. Their sample overlapped the present one in only one quasar, PG1704+518 (3C351; Figure 31). This quasar shows a variation in B of $\sim$0.5 mag which is reflected in a comparable variation in the near-infrared wavelengths. All the quasars in Netzer et al's sample varied during their six year survey, some by as much as 3 mag (maximum variation) but half of them by 0.2 to 0.4 mag. Presumably, the variations found in Netzer et al's observations represent an indication of the nonthermal fluctuations present in a sample of nonthermal quasars and as such is interesting to compare with the present survey.

As a robust measure of the variability, Netzer et al. (1996) tabulated the "median variability" of their survey. The "median variability" is defined as the median of the absolute value of the peak to peak magnitude difference taken over the run of all measurements of a quasar in a particular wavelength band. The distributions of the median variability provide a convenient tool to compare a presumably nonthermal population with the infrared sample.

Figure 10 (top) shows the distributions of the median variability of the radio loud and radio quiet sub-samples as observed in the present survey at 10.6 μm. The distributions of the median variabilities of the shorter wavelength near-infrared observations agree qualitatively with those shown in Figure 10. Although there is a slight tendency at 10.6 μm for a higher median variability among the radio loud quasars than among the radio quiet quasars, there is essentially no difference between the two groups. A further comparison is made in Figure 10 (bottom) which shows the median variability of the present 10.6 μm measurements as compared with that of the median variability obtained by Netzer et al. (1996) in the B-wavelength band (0.44 μm). Although there is no significant overlap between Netzer et al.'s sample and the present sample, and this median does not account for the larger uncertainties in the 10.6 μm observations or the difference in sampling frequency, there is no strong difference between the two distributions. In particular, the medians have comparable amplitudes, and the infrared variations do not show the decreased amplitude expected from thermal emission on the simple model described above.

The variations observed by Netzer et al. (1996) are almost certainly nonthermal. Thus we take the similarities present in Figures 10 as evidence that a nonthermal component is present in the 10.6 μm emission of both radio loud and radio quiet quasars.

5.4. Structure function

Structure function analysis is useful in discussing variability of unevenly sampled data sets. The structure function is discussed in the context of astronomical variability by e.g., Simonetti, Cordes & Heeschen (1985), Hughes, Aller & Aller (1992), Press, Rybicki & Hewitt (1992) and Smith et al. (1993). If the observations are made at time intervals which are short compared to true variations in the quasar flux, the structure function for short time lags reflects the measurement noise in the sample. The structure function for large

lags characterizes the low frequency variations in the quasar flux.

The following discussion closely follows that of Press et al. (1992). At each wavelength, a lag $\tau_{i,j}$ was computed for each pair of observations:

$$\tau_{i,j} =\mid \tau_i - \tau_j \mid$$

A one-point estimate of the structure function, $sf_{i,j}$, was calculated for each lag:

$$sf_{i,j} \equiv (m_i - m_j)^2 - \epsilon_i^2 - \epsilon_j^2$$

where m_i and m_j are the magnitudes observed at a specific wavelength at times τ_i and τ_j, and ϵ_i and ϵ_j are the quoted standard deviations of the measurement. The structure function estimates were sorted by their lags, and then binned so that each bin contained at least 50 individual estimates and lags. The lags and the one point estimates in each bin were finally averaged. These averages for the 10.6 μm observations of all the 25 quasars in the sample are shown in Figure 11. The figure indicates a difference in the behavior of radio loud quasars and radio quiet quasars although the large amplitude around two to three years in the radio loud quasars is mainly the result of one quasar (PG2209+184).

Although the structure function analysis does not directly address the question of the nature of the emission around 10 μm from quasars, the structure function does give clues as to the nature of the near-infrared emission from PG1226+023, the best studied of the quasars. The structure functions for PG1226+023 at all the five wavelengths are shown in Figure 12. At the three shorter wavelengths, the structure function clearly shows peaks at lag times separated by about a decade. As a check that these peaks are not an artifact of the processing, a similar analysis to that described above was carried out on data which were artificially scrambled in time, but maintained the sampling pattern and the intensity levels

of the original observations. As a result of these checks, we conclude that the processing is not responsible for the variations observed and that the structure functions reflect a real property of the quasar.

As pointed out by e.g., Smith et al. (1993), a sinusoidal variation in the fluxes gives a sinusoidal variation of similar period in the structure function such as seen in Figure 12. Thus, the almost periodic appearance of the structure function indicates a quasi-periodic fluctuation in the near- infrared emission of the quasar. The maximum near ten years in the lag indicates that an oscillatory mechanism with a period near a decade is present in the nonthermal central engine. A maximum was often seen in the visible structure functions studied by Smith et al. at lags between five and ten years and a double humped profile with a period roughly a decade was observed in the quasar 1318+290 leading to the speculation that the "periodic" behavior is a feature of the nonthermal engine of the radio loud quasars. Smith et al., however, do not call attention to any striking behavior in PG1226+023 and thus the behavior seen in Figure 12 may be restricted to emission in a rather small wavelength interval.

The sinusoidal behaviour appears to be missing from the 3.7 μm observations of PG1226+023. Numerical simulations of the data were made where a sine wave with an amplitude of 0.5 mag and a period of 11 years was sampled as the real data were, given random deviations proportional to the actual uncertainties and assigned the uncertainties of the real data. These simulations were able to reproduce the data and structure functions at all the measured wavelengths, including 3.7 and 10.6 μm, quite realistically. Thus we conclude that the absence of an obvious signature can be a result of the sampling and uncertainties in the data and that the observations are consistent with an underlying sinusoidal variation in this quasar at all the observed wavelengths.

The roughly periodic nature of the structure function present for PG1226+023 is not

a universal feature in all the quasars or even all the radio loud quasars. As indicated by Figure 11, however, the maxima near a decade seem to be present more often among the near-infrared observations of the radio loud than among the radio quiet quasars.

6. Conclusions

There is no single set of observations which, on the basis of their temporal variations, can unambiguously demonstrate that nonthermal emission dominates the 10 μm peak of any radio quiet quasar. The strongest case is that of PG1545+47 which shows apparently correlated variations on time scales less than decades with similar amplitudes at all the infrared wavelengths. In this object, at least, the most simplistic model of purely thermal emission cannot unambiguously explain the observations. Unfortunately, PG1545+47 is the lowest luminosity quasar of the sample and the predicted lack of variability in thermal emission from dust around quasars depends strongly on the luminosity. It is also always possible, indeed almost certainly true, that special geometries or constituents, coupled with the low luminosity, can conspire to allow thermal emission to vary on time scales less than a decade. The similarity of the median variability of the 10.6 μm observations and that of the near-infrared observations and the visible observations of Netzer et al. (1996) (Figure 10) argues that some of the 10.6 μm radiation is nonthermal. Thus some nonthermal emission is apparently present in some radio quiet quasars, i.e., both thermal radiation from dust and nonthermal radiation contribute to the "infrared bump".

7. Acknowledgements

A project of several decades duration cannot be contemplated without the support and help of a large number of people. We thank Lee Armus, Eric Becklin, Jay Elias, James

Graham, Todd Hunter, Jon Kawamora , David Shupe, Tom Soifer and Alycia Weinberger as well as the night assistants Rick Burruss, Juan Carrasco, Gene Hancock, Skip Staples and Gary Tuton and the entire staffs of Palomar and Mt. Wilson Observatories for help obtaining these data. We acknowledge helpful discussions with Lee Armus, Peter Barthel, Roger Blandford, David Hogg, Marcia Neugebauer, Sterl Phinney, Annila Sargent, Tom Soifer and Alycia Weinberger. Caltech, NSF and NASA have supported us over the years.

A. Appexdix

The observations of the 21 quasars not shown in Figures 2–5 are given in Figures 13–33 in the format of Figure 2.

REFERENCES

Bahcall, J. N., Kirhakos, S., Saxe, D. H. & Schneider, D. P. 1997, ApJ, 479, 642

Bloom, S. D., Marscher, A. P., Gear, W. K., Teraesranta, H., Valtaoja, E., Aller, H. D. & Aller, M. F. 1994, AJ, 106, 398

Bregman, J. N. 1994, in Multi-Wavelength Continuum Emission of AGN, IAU Symposium 159, Vol. ed. Courvoisier, T. J.-L. and Blecha, A. (Geneva, Switzerland, Dordrecht, Boston, Kluwer, Academic Press), p. 5

Courvoisier, T. J., Robson, E. I., Blecha, A., Bouchet, P., Hughes, D. H., Krisciunas, K. & Schwarz, H. E. 1988, Nature, 335, 330

Cutri, R. M., Wisniewski, W. Z., Rieke, G. H. & Lebofsky, M. J. 1985, ApJ, 296, 423

Draine, B. T. & Lee, H. M. 1984, ApJ, 285, 89

Elias, J. H., Frogel, J. A., Matthews, K. & Neugebauer, G. 1982, AJ, 87, 1029

Elvis, M.S. et al.1994, ApJ, 95, 1

Hoffleit, D. 1964, Catalogue of Bright Stars (New Haven, Connecticut, Yale University Observatory)

Hughes, P. A., Aller, H. D. & Aller, M. F. 1992, ApJ, 396, 469

Kukula, M. J., Dunlop, J. S., Hughes, D. H. & Rawlings, S. 1998, MNRAS, 297, 366

Kellermann, K. I., Sramek, R. A., Schmidt, M., Green, R. F. & Shaffer, D. B. 1994, AJ, 108, 1163

Mathis, J. S., Rumpl, W. & Nordsieck, K. H. 1977, ApJ, 217, 425

McLeod, K. K. & Rieke, G. H. 1994a, ApJ, 420, 58

McLeod, K. K. & Rieke, G. H. 1994b, ApJ, 431, 137

Netzer, H., et al. 1996, MNRAS, 279, 429

Neugebauer, G., Green, R. F., Matthews, K., Schmidt, M., Soifer, B. T. & Bennett, J. 1987, ApJ, 63, S615

Neugebauer, G., Matthews, K. & Armus, L. 1995, ApJ, 455, L123

Neugebauer, G., Soifer, B. T., Matthews, K. & Elias, J. H. 1989, AJ, 97, 957

Press, W. H., Flannery, B. P., Teukolsky, S. A. & Vetterling, W. T. 1985, Numerical Recipes The Art of Scientific Computing Cambridge University Press)

Press, W. H., Rybicki, G. B. & Hewitt, J. N. 1992, ApJ, 385, 404

Rieke, G. H. & Lebofsky, M. J. 1979, ARA&A, 17, 477

Robson, E. I., et al. 1983, Nature, 305, 194

Robson, E. I., et al. 1993, MNRAS, 262, 249

Sanders, D. B., Phinney, E. S., Neugebauer, G., Soifer, B. T. & Matthews, K. 1989, ApJ, 347, 29

Schmidt, M. & Green, R. F. 1983, ApJ, 269, 352

Simonetti, J. H., Cordes, J. M. & Heeschen, D. S. 1985, ApJ, 296, 46

Smith, A. G., Nair, A. D., Leacock, R. J. & Clements, S. D. 1993, AJ, 105, 437

Ulrich, M.-H., Maraschi, L. & Urry, C. M. 1997, ARA&A, 35, 445

Wilkes, B. J., Hooper, E. J., McLeod, K. K., Elvis, M. S., Impey, C. D., Lonsdale, C. J., Malkan, M. A. & McDowell, J. C. 1998, in The Universe as Seen by ISO, Vol. SP-427, Paris, ESA Special Publication Series, preprint

Fig. 1.— (left) A histogram of the bolometric luminosities, as described in the text, of the quasars in the sample is shown. (right) A histogram of the redshifts of the quasars in the sample is given. The redshifts and bolometric luminosities are from Sanders et al. (1989).

Fig. 2.— The observations of the quasar PG1226+023 at (from the bottom to the top) 1.27, 1.65, 2.23, 3.7 and 10.6 μm are given as magnitude differences from the long term weighted average of the magnitudes measured in this study at that wavelengh. The ordinate range, which is the same at each wavelength, is adjusted to include the largest excursions in any band and is labeled in the bottom, middle and top panels. The dashed lines indicate a weghted linear fit to all the magnitudes obtained in this study. For each band, the long term weighted average magnitude determined in this study and the reduced χ^2 are given to the right of the figure.

Fig. 3.— The same as Figure 2, but for PG2209+184.

Fig. 4.— The same as Figure 2, but for PG1501+106.

Fig. 5.— The same as Figure 2, but for PG1535+547.

Fig. 6.— The magnitude change at one wavelength versus that at another wavelength is shown for the observations of PG1226+023. The differences in the observations at the two wavelengths given in the upper left of each panel (upper—ordinate, lower—abscissa) are compared. Solid dots indicate that the time interval between measurements was less than five years, while crosses indicate longer intervals. Only those cases where subsequent observations were made on the same nights at two wavelengths are presented so all the data taken are not included, and so these data are more concentrated to the time since 1988. In those cases where the changes are apparently correlated, formally where the significance

level at which the null hypothesis of zero correlation is disproved is less than 5% (see e.g., Press et al. 1985), a dashed line indicating the best fit to the correlation is shown.

Fig. 7.— The same as Figure 6, but for PG1535+547.

Fig. 8.— The same as Figure 6, but for PG1351+640.

Fig. 9.— (top) Responses at 2.23, 3.7 and 10.6 μm to a step increase of the central source from 1.4×10^{12} to $1.8\times10^{12} L_{\odot}$ are shown for silicate grains in the model described in the text. The grain density is assumed to decrease with radius from the central source as $(\text{radius})^{-2}$. (bottom) Expected 10–90% rise times are shown for the observations at 2.23, 3.7 and 10.6 μm if, in the model described in the text, the luminosity of the central source increases by 50%. The central luminosities included in the figure span the luminosity range of the quasars in the sample and the predictions are shown for both silicate (solid lines) and graphite grains (dashed lines) in the simple thermal model described in the text.

Fig. 10.— (top) A histogram is given of the median variability, as defined in the text, of the 10.6 μm observations in this study. The sample is divided into radio quiet (single hatches) and radio loud (cross hatches) quasars.
(bottom) A comparison is shown of the median variability measured at 10.6 μm in this study (cross hatched bars) and that measured in the B band (0.44 μm) by Netzer et al. (1996) for a sample of radio loud quasars (single hatched bars).

Fig. 11.— The average structure functions for the 10.6 μm observations of all 25 of the quasars in this sample are shown. The vertical error bars assigned to each point on a structure function are the standard deviations in the means of each bin, and thus reflect the spread in the estimates making up one bin, while the error bars in the lags are arbitrarily sized to extend from one to three quarters of the time interval between adjacent lag times. The radio quiet quasars are distinguished from radio loud quasars as indicated; the measurements of

PG1226+023 were so much more numerous than those of the other objects that they were treated separately.

Fig. 12.— The structure functions at all five wavelengths for the quasar PG1226+023 are given. The error bars have the same meaning as those in Figure 11. The amplitude scale for each wavelength is different.

Fig. 13.— The same as Figure 2, but for PG0007+106.

Fig. 14.— The same as Figure 2, but for PG0026+129.

Fig. 15.— The same as Figure 2, but for PG0050+124.

Fig. 16.— The same as Figure 2, but for PG0157+001.

Fig. 17.— The same as Figure 2, but for PG0804+761.

Fig. 18.— The same as Figure 2, but for PG0844+349.

Fig. 19.— The same as Figure 2, but for PG1119+120.

Fig. 20.— The same as Figure 2, but for PG1211+143.

Fig. 21.— The same as Figure 2, but for PG1229+204.

Fig. 22.— The same as Figure 2, but for PG1351+640.

Fig. 23.— The same as Figure 2, but for PG1402+261.

Fig. 24.— The same as Figure 2, but for PG1411+442.

Fig. 25.— The same as Figure 2, but for PG1426+015.

Fig. 26.— The same as Figure 2, but for PG1440+356.

Fig. 27.— The same as Figure 2, but for PG1613+658.

Fig. 28.— The same as Figure 2, but for PG1617+175.

Fig. 29.— The same as Figure 2, but for PG1634+706.

Fig. 30.— The same as Figure 2, but for PG1700+518.

Fig. 31.— The same as Figure 2, but for PG1704+608.

Fig. 32.— The same as Figure 2, but for PG2130+099.

Fig. 33.— The same as Figure 2, but for PG2302+029. In this figure only, the range of the ordinate scale has been truncated below the extremes of the 10.6 μm uncertainties.

Table 1. Sample

Object	radio type[a]	redshift	$\log[L_{bol}(L_{\odot})]$
PG0007+106	L	0.089	12.24
PG0026+129	Q	0.142	12.49
PG0050+124	Q	0.061	12.20
PG0157+001	Q	0.164	12.78
PG0804+761	Q	0.100	12.56
PG0844+349	Q	0.064	11.86
PG1119+120	Q	0.049	11.72
PG1211+143	L	0.085	12.44
PG1226+023	L	0.158	13.44
PG1229+204	Q	0.064	11.84
PG1351+640	Q	0.087	12.14
PG1402+261	Q	0.164	12.36
PG1411+442	Q	0.089	11.94
PG1426+015	Q	0.086	12.13
PG1440+356	Q	0.077	11.98
PG1501+106	Q	0.036	11.82
PG1535+547	Q	0.038	11.44
PG1613+658	Q	0.129	12.26
PG1617+175	Q	0.114	12.11
PG1634+706	Q	1.334	14.24
PG1700+518	Q	0.292	13.08
PG1704+608	L	0.371	13.02
PG2130+099	Q	0.061	11.96

Table 1—Continued

Object	radio type[a]	redshift	$\log[L_{bol}(L_{\odot})]$
PG2209+184	L	0.070	12.00
PG2302+029	Q	1.044	13.37

[a] "Q" – radio quiet; "L" – radio loud